Effect of back cavity configuration on performance of elastic panel acoustic liner with grazing flow

Garret C.Y. Lam, Randolph C.K. Leung, Harris K.H. Fan, Yves Aurégan

Effect of Back Cavity Configuration on Performance of Elastic Panel Acoustic Liner with Grazing Flow

Garret C.Y. Lam[a], Randolph C.K. Leung[a,*], Harris K.H. Fan[a], Yves Aurégan[b]

[a] *Department of Mechanical Engineering, The Hong Kong Polytechnic University, Hung Hom, Kowloon, Hong Kong, P. R. China*

[b] *Laboratoire d'Acoustique de l'Université du Maine, UMR CNRS 6613, Av. O. Messiaen, 72085 LE MANS Cedex 9, France*

Abstract

This paper reports a numerical study of noise mitigation mechanism of elastic panel liner comprising an elastic panel and a cavity beneath exposed to grazing flow with time-domain direct aeroacoustic simulation seamlessly coupled with panel dynamics. The effect of cavity configuration on the acoustic behavior of liner is investigated through a parametric study which covers variations of cavity depth, panel length and cavity shape. Extensive cross spectral analysis of numerical results of all variations reveal that wave canceling due to destructive interference with the incident acoustics in downstream duct is confirmed the major noise mitigation mechanism. Another mechanism is the high order mode re-radiation from the panel in response to incident acoustics. The cavity configuration effectively modifies its acoustic distribution inside as well as the propagation speed of excited panel flexural waves. All the observations reveal that cavity configuration plays an essential role in identified noise mitigation mechanisms. A new elastic panel liner with absorptive material attached to cavity side is proposed. Its configuration is confirmed to effectively relieve the acoustics inside the cavity leading to prominent enhancement of noise mitigation. The achievement shows that back cavity configuration is an important design consideration for elastic panel liner mitigation performance.

Keywords: Acoustic liner, Elastic panel, Cavity

PACS: 43.28.–g, 43.28.Py, 43.55.Dt

*Corresponding author

Email addresses: garret.lam.hk@connect.polyu.hk (Garret C.Y. Lam), mmrleung@polyu.edu.hk (Randolph C.K. Leung), harris@connect.polyu.hk (Harris K.H. Fan), yves.auregan@univ-lemans.fr (Yves Aurégan)

1. Introduction

Traditional acoustic liner using absorptive materials is commonly adopted for passive noise mitigation inside an engineering flow duct systems. Although these liners perform well at mid- to high-frequency ranges, they are not effective in reducing the low-frequency noise due to the characteristics of their dissipation mechanism in noise mitigation [1]. Thus, it usually requires a very bulky liner for low frequency applications. To cope with such limitation, researchers are still working on developing various ideas such as micro-perforated plate [2] and slow sound device [3] to improve the mitigation of low-frequency noise. Previous studies have also demonstrated the great potential of using an elastic panel as a liner for noise mitigation in a flow duct system. Huang [4] studied the acoustics of such elastic panel (EP) liner in the absence of grazing flow and found that it could be designed to achieve reduction over quite broad range of low frequency. Recently, dielectric elastomer membrane has been attempted as the elastic panel [5] to mitigate noise. By applying voltage control across such membrane, the transmission loss can be tuned to desired frequency range. This further extends the applicability of such concept in noise mitigation.

The early works related to EP liner often ignored the external pressure perturbation acting on the panel [4, 6]. Constant pressure is assumed on the side of elastic panels exposed to duct exterior. In other words, they assumed that the panels do not transmit acoustics outside the duct. Following Doak's work [7], the vibrating velocity of panels were treated as acoustic source to determine the induced acoustic pressure fluctuation in the duct. For example, Choi and Kim [6] studied the acoustic waves propagation in a duct mounted with an finite elastic panel. They derived the phase speeds of these waves as a function of panel properties and the acoustic re-radiation from the panel in a stagnant fluid. Nevertheless, in practical implementation of EP liner, the elastic panel inevitably needs shielding from the noise breaking out to duct exterior and protection without hindering its vibration. A simple method is to cover the elastic panel at the surface exposed to the surroundings. In this way, the space between the cover and the panel creates a cavity. This cavity and the panel become a coupled system which determines the acoustic performance of EP liner. Therefore, subsequent works [8, 9, 10] started to investigate the acoustic performance of such system theoretically and numerically. In their theoretical studies, they applied modal analysis and treated the panel vibration as a series of *in vacuo* modes. They then adopted Doak's work to evaluate the acoustic generation by the vibrating panel to duct interior. The acoustic effect of the cavity has been approximated by superposing

acoustical reflections of cavity vertical walls and acoustic generation of the panel at plane wave mode only. An "optimal" EP liner was attempted by searching in a range of parameters such as geometric parameters, material and panel tension. In addition to the ignorance of grazing flow effect, high order cavity acoustic modes are also ignored. Later an experimental and numerical work of EP liner with a cavity was also carried out [11] emphasizing the effect of the mean flow speed and the panel tension. The effect of mean grazing flow speed was further extended up to Mach number $M = 1.2$ in a recent work [12], which assumes an inviscid flow as those in previous works. This assumption was relaxed in a subsequent work [13].

In the original design of EP liner for noise mitigation [4], when acoustic waves pass through an EP liner in a flow duct, they excite the elastic panel to vibrate and induce flexural waves on the panel which are then dissipated by structural damping. As a result, the acoustical energy is lost via this process. This is the first mechanism of noise mitigation by EP liner. During the passage of acoustics over the liner, another noise mitigation mechanism also comes into action. The sudden distensibility at the panel slows down the waves above the liner [6]. The mismatch of wave speeds leads to reflection of the acoustic waves and their scattering at the rigid corner of the liner. These newly generated acoustic waves, termed re-radiated waves, propagate with the original incident wave downstream, causing stop band and passing band depending on the frequencies of the waves. In the literature [4, 6, 9, 11, 10, 14], this reduction is treated as a result of acoustic reflection by the EP liner. The authors interpreted such reflection as the interference between the acoustics generated from different *in vacuo* modes of panel only in their modal analysis. Therefore, they focused on the modal resonances of panel and regarded them as the dominant process responsible for the noise mitigation. Nevertheless, according to their mathematical formulation, the transmitted waves are the superposition of incident acoustics and re-radiated waves by the panel in the downstream branch. Weakened transmitted waves are the consequence of destructive interference between these two waves in the downstream duct. Therefore, this reduction mechanism is actually wave canceling in nature, rather than acoustic reflection by panel as suggested in the literature. Up to this moment, these two are the noise mitigation mechanisms of EP liner found in the literature.

Despite the achievements of the aforementioned works, the design of EP liner for noise mitigation in use with a practical system remains difficult. The works cast the panel vibration into a series of *in vacuo* modes termed as modal resonances which actually assume the synchronization of the opposite propagating flexural

waves. This may not be always true in the process especially when a grazing flow exists, so these modes do not truly describe the actual propagation of the induced flexural waves on panel. They have also focused primarily on the transmission loss, which represents only part of the acoustic behavior of EP liner. Other acoustic behaviors such as reflection and absorption received little attention in these works. This leaves some unexplained observations. For instance, local peak frequencies of transmission loss always deviate from those of panel vibrating speed with up to 20% in their results. The actual noise mitigation mechanisms are still vague, not to mention if other noise mitigation mechanism exists. Another component of EP liner whose influence remain unclear is the cavity beneath the panel. As those works considered only plane wave acoustic modes inside cavity, it is highly probable that a non-uniform vibrating source such as panel generates high order acoustic modes particularly near the panel in cavity. Only a few works investigates the effect of cavity on the acoustic performance without this assumption. For example, Du et al. [15] investigated the change of transmission loss (TL) with different shapes of the cavity without grazing flow. The trend of TL changes completely with the shape of cavity changing from rectangular cavity to other irregular shape. This indicates an important role of cavity in determining the acoustic performance of EP liner. However, the role of the cavity on the acoustic performance of such liner remains uncertain under a grazing flow. The aims of the present study are three folds. The first is to give a detailed study of the noise mitigation mechanisms of EP liner. The second is to explore the role of the cavity on the acoustic performance of EP liner. This involves numerically examining the acoustic behaviors of the elastic panel under different cavity sizes and shapes in the presence of a grazing flow. This situation may shed light on any flow and acoustics or structural interaction that affects the performance of EP liner. Finally, modification of cavity configuration in the liner will be explored for enhancing noise mitigation.

This paper is organized as follows. Section 2 describes the formulation of the problem including the numerical method adopted and its setup. Section 3 shows the results and we first compare the acoustic behaviors of EP liner with rectangular cavity of different sizes, followed by those at various cavity shape, in which length of the cavity base is changed. Next, a new concept of utilizing the cavity will be explored to further enhance the EP liner mitigation performance. Finally, we will conclude the findings in the last section.

2. Formulation of the problem

2.1. Numerical approach

Since the noise mitigation of EP liner for flow duct system involves the interplay between the incident acoustics, flow and panel structural vibration, it requires an approach that is capable of resolving all the contributed physical processes. Most of the previous numerical works adopt a frequency-domain approach which may not reveal the nonlinear details of noise mitigation mechanism easily. In the present study, we adopt Direct Aeroacoustic Simulation (DAS) approach combined with a monolithic approach for incorporating the panel structural dynamics into time marching of solution [16, 17]. DAS is a time-domain numerical approach which solves the compressible Navier-Stokes (N-S) equations and the equation of state simultaneously. It inherently resolves the interplay between the flow dynamic and the acoustic solutions in a seamless manner. DAS has been successfully applied in studying the aeroacoustics of duct flow using the Conversation Element and Solution Element (CE/SE) method [18, 19]. The monolithic approach that couples with a finite difference structural solver guarantees the instantaneous information exchange between the aeroacoustics and structural dynamics at every time step. In other words, the flow dynamics, acoustics and structural dynamics of panel are solved simultaneously at every time step. This ensures the correct interaction between all the solutions. Readers can refer to Ref. [17] for the detailed implementation of the current approach. Only the governing equations will be described in this paper.

The present aeroacoustics is governed by the N-S equations and the equation of state (Eq. 1). The acoustics of interest is at very low frequency compared to the duct cut-off frequency. It is expected that two dimensional flow behaviors and acoustic plane wave are dominant in the overall mitigation physics [11]. Thus, two dimensional form of N-S equations and one dimensional structural panel equation are adopted. We denote the dimensional quantities with the hat $\widehat{\ }$, those without as their normalized counterparts and the subscript ∞ as the inlet quantities. Taking the reference scales of half-duct width $\widehat{H}$, ambient speed of sound $\widehat{c_\infty}$, density $\widehat{\rho}_\infty$, dynamic pressure $\widehat{\rho}_\infty \widehat{c}_\infty^2$, temperature $\widehat{T}_\infty$ and viscosity $\widehat{\mu}_\infty$, the normalized N-S equations can be written in strong conservation form as

$$\frac{\partial \boldsymbol{U}}{\partial t} + \frac{\partial \left(\boldsymbol{F} - \boldsymbol{F_v}\right)}{\partial x} + \frac{\partial \left(\boldsymbol{G} - \boldsymbol{G_v}\right)}{\partial y} = 0, \tag{1}$$

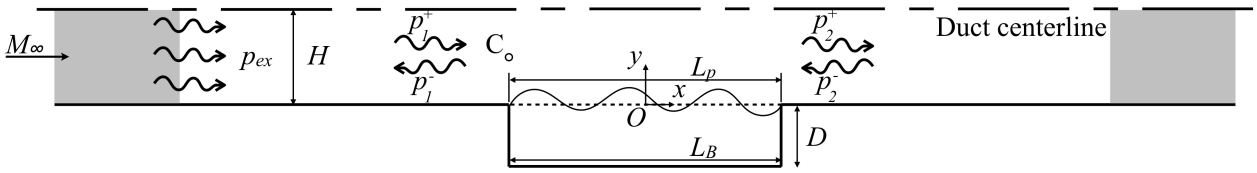

Figure 1: Schematics of computational domain. p_1^+ and p_1^- denote the wave propagating along $+x$ and $-x$ directions in upstream branch respectively. Similar definitions of p_2^+ and p_2^- are applied for downstream branch.

where $\boldsymbol{U} = [\rho, \rho u, \rho v, \rho E]^{\mathrm{T}}$, $\boldsymbol{F} = \left[\rho u, \rho u^2 + p, \rho uv, (\rho E + p)\, u\right]^{\mathrm{T}}$, $\boldsymbol{G} = \left[\rho u, \rho uv, \rho v^2 + p, (\rho E + p)\, v\right]^{\mathrm{T}}$, $\boldsymbol{F_v} = [0, \tau_{xx}, \tau_{xy}, \alpha_x]^{\mathrm{T}} M_\infty / Re_\infty$, $\boldsymbol{G_v} = [0, \tau_{xy}, \tau_{yy}, \alpha_y]^{\mathrm{T}} M_\infty / Re_\infty$ with u and v being the velocities in x and y directions respectively, $\alpha_x = \tau_{xx} u + \tau_{xy} v - q_x$, $\alpha_y = \tau_{xy} u + \tau_{yy} v - q_y$, shear stresses $\tau_{xx} = \frac{2}{3}\mu\left(2\frac{\partial u}{\partial x} - \frac{\partial v}{\partial y}\right)$, $\tau_{xy} = \mu\left(\frac{\partial u}{\partial y} + \frac{\partial v}{\partial x}\right)$, $\tau_{yy} = \frac{2}{3}\mu\left(2\frac{\partial v}{\partial y} - \frac{\partial u}{\partial x}\right)$, internal energy $E = \frac{p}{\rho(\gamma-1)} + \frac{u^2+v^2}{2}$, pressure $p = \frac{\rho T}{\gamma}$, heat fluxes $q_x = -\frac{\mu}{(\gamma-1)Pr_\infty}\frac{\partial T}{\partial x}$, $q_y = -\frac{\mu}{(\gamma-1)Pr_\infty}\frac{\partial T}{\partial y}$, the specific heat ratio $\gamma = 1.4$, inlet uniform flow Mach number $M_\infty = \widehat{U}_\infty / \sqrt{\gamma \widehat{R} \widehat{T}_\infty}$, specific gas constant $\widehat{R} = 287.058 J/\left(kg{\cdot}K\right)$ for air, Reynolds number $Re_\infty = \widehat{\rho}_\infty \widehat{U}_\infty \widehat{L} / \widehat{\mu}_\infty$ and Prandtl number $Pr_\infty = \widehat{c_{p,\infty}} \widehat{\mu}_\infty / \widehat{k}_\infty = 0.71$.

The structural governing equation of a homogeneous panel is expressed in normalized form as

$$E_b \frac{\partial^4 \delta}{\partial x^4} - (\sigma_p + N)\frac{\partial^2 \delta}{\partial x^2} + \rho_p h_p \frac{\partial^2 \delta}{\partial t^2} + C\frac{\partial \delta}{\partial t} = \triangle p, \tag{2}$$

where δ is the panel deflection, the applied tension on the panel $\sigma_p = \widehat{\sigma_p} / \left(\widehat{\rho_\infty} \widehat{c_\infty}^{\,2} \widehat{H}^2\right)$, the tangential internal stress induced by stretching $N = (E_p h_p / 2L_p) \int_0^{L_p} \left(\partial\delta/\partial x\right)^2 dx$, Young's modulus $E_p = \widehat{E_p} \widehat{c_\infty}^{\,2} / \left(\widehat{\rho_\infty} \widehat{H}^4\right)$, h_p is the thickness of the panel, L_p is the length of the panel, bending stiffness $E_b = E_p h_p^3 / 12\left(1 - \nu^2\right)$, υ is Poisson's ratio of the panel, ρ_p is the density of the panel, $C\left(= \widehat{C} / \widehat{\rho_\infty} \widehat{c_\infty}\right)$ is the structural damping coefficient of the panel and $\triangle p$ is the pressure difference across both sides of the panel.

2.2. Numerical setup

Fig. 1 illustrates the computational domain in the study. A uniform flow with Mach number $M_\infty = 0.045$ enters a duct of width $2H$ from the right inlet and acoustic excitation with frequency range $0.0029 < f < 0.25$ is introduced at the upstream branch corresponding to 20 Hz $< f <$ 1700 Hz in a duct of width $2\widehat{H} = 100$ mm. The acoustic excitation is in the form $p_{ex}(t) = |p_{ex}| \sum_m \sin\left(\omega_m t + \varphi_m\right) = p_1^+$, where ω_m and φ_m are the m-th excited frequency and random phase respectively. The choice of inlet Mach number follows an early

Configuration	S1	S2	S3	S4	T1	T2	C1	C2	C3	C4
D	2	1	2	1	0.2	0.2	2	2	2	2
L_p	10	10	5	5	10	5	10	10	10	10
L_B	10	10	5	5	10	5	5	7.5	12.5	15
$\triangle x_{duct}$	0.2	0.2	0.1	0.1	0.2	0.1	0.2	0.2	0.2	0.2
$\triangle y_{duct}$	0.033	0.033	0.033	0.033	0.02	0.02	0.033	0.033	0.033	0.033
$\triangle x_{ca,max}$	0.2	0.2	0.1	0.1	0.2	0.1	0.2	0.2	0.2	0.2
$\triangle x_{ca,min}$	0.2	0.2	0.1	0.1	0.2	0.1	0.1	0.15	0.25	0.3
$\triangle y_{ca}$	0.033	0.033	0.033	0.033	0.02	0.02	0.033	0.033	0.033	0.033

Table 1: Variation of parameters and mesh settings in the present study.

experimental work [11] whose results have been successfully reproduced in the numerical study of Fan et al. [17]. An elastic panel of length L_p is flush mounted on the lower duct wall starting at $x = -L_p/2$ and a cavity of depth D lies underneath. Both ends of panel are simply supported. Structural damping effect of the panel is ignored in this study, i.e. $C = 0$. The grey areas attached to the inlet and exit of duct physical domain are exponentially grid-stretched buffer zones for elimination of erroneous numerical reflection. Outlet is set with a non-reflecting boundary condition and the top boundary is a symmetric boundary condition. All the walls including the elastic panel are prescribed with no-slip boundary condition but those in the upstream buffer zones are prescribed as sliding walls. Table 1 lists the variations of $L_p\,(= 5, 10)$, $D\,(= 0.2, 1, 2)$ and the length of the cavity base $L_B\,(= 5, 7.5, 12.5, 15)$ in the parametric study and their corresponding mesh parameters. The meshes consist of triangular elements divided from uniform quadrilateral mesh, whose sizes are $\triangle x$ and $\triangle y$ in x- and y- direction respectively. The subscripts "*duct*" and "*ca*" in the table denote the duct and the cavity respectively. In all calculations, time-stationary flow solutions are firstly obtained without acoustic excitation. Then calculations with time increment $\triangle t = 0.0025$ proceed for a duration of 3400 normalized time units. Plane wave assumption is still valid in these two branches as the highest exciting frequency is well below the cut-off frequency $f_{cutoff} = 0.5$. All analyses discussed hereafter are calculated from the time-stationary solutions covering the last two periods of the lowest exciting frequency ($2720 \leq t \leq 3400$). In Fig. 1, p_1^+ and p_1^- denote the acoustic wave propagating along $+x$ and $-x$ directions in upstream branch respectively. Similar definitions are applied to p_2^+ and p_2^- for downstream branch.

n-th Mode	1	2	3	4	5	6	7	8
$f_{L_p=5,n}$	0.051	0.114	0.177	0.241				
$f_{L_p=10,n}$	0.022	0.051	0.082	0.114	0.145	0.177	0.209	0.241

Table 2: Theoretical natural frequencies $f < 0.25$ for all panels in the study.

3. Results & Discussions

In the following analysis, the acoustic results in the upstream and downstream branches of the panel are obtained from $-10 < x < -5$ and $5 < x < 10$ with a increment of 0.5 at $y = 0.5$ respectively. Acoustic pressure is calculated by $p'(x,y,t) = p(x,y,t) - \overline{p(x,y,t)}$ where the term with over-bar is the time averaged total pressure [16]. Multiple microphone method [20] is then applied to discern the acoustic pressure into waves propagating along $\pm x$ directions, e.g. p_1^+ and p_1^- in Fig. 1. Since the noise mitigation of EP liner involves the vibration of elastic panel, it is beneficial to compare the results with the panel natural frequencies. Following the derivations given in Ref. [21] and [22], the n-th natural frequencies of the elastic panels of length L_p loaded in stagnant flow $\left(f_{L_p,n}\right)$ are estimated by the following dimensionless formula,

$$f_{L_p,n} = \frac{n}{2L_p}\sqrt{\frac{n\pi\sigma_p}{n\pi\rho_p h_p + L_p}}. \tag{3}$$

Table 2 lists for all modes below the maximum excitation frequency for $L_p = 5$ and $L_p = 10$.

In this section, the results with rectangular cavity S1 to T2 will be presented first and the noise mitigation mechanism will also be detailed with analyses of these results. The results of non-rectangular cavity C1 to C4 will be discussed later.

3.1. Rectangular Cavity

Fig. 2 shows the transmission losses $TL = 20\log_{10}\left(p_1^+/p_2^+\right)$ of EP liners for cases S1 - S4 and T1 - T2. Case S1 is a replica of previous experimental work [11], whose results are reproduced as black circles in Fig. 2a. The close matching between case S1 and with experimental results indicates the successful capture of the acoustic behavior of EP liner using the present numerical method. It also indicates that panel structural damping is insignificant in these cases. In general, TLs are very low at frequency $f < f_{L_p,1}$. In this frequency band the panel appears insensitive to acoustic excitation suggesting that EP liner is not effective at all. In

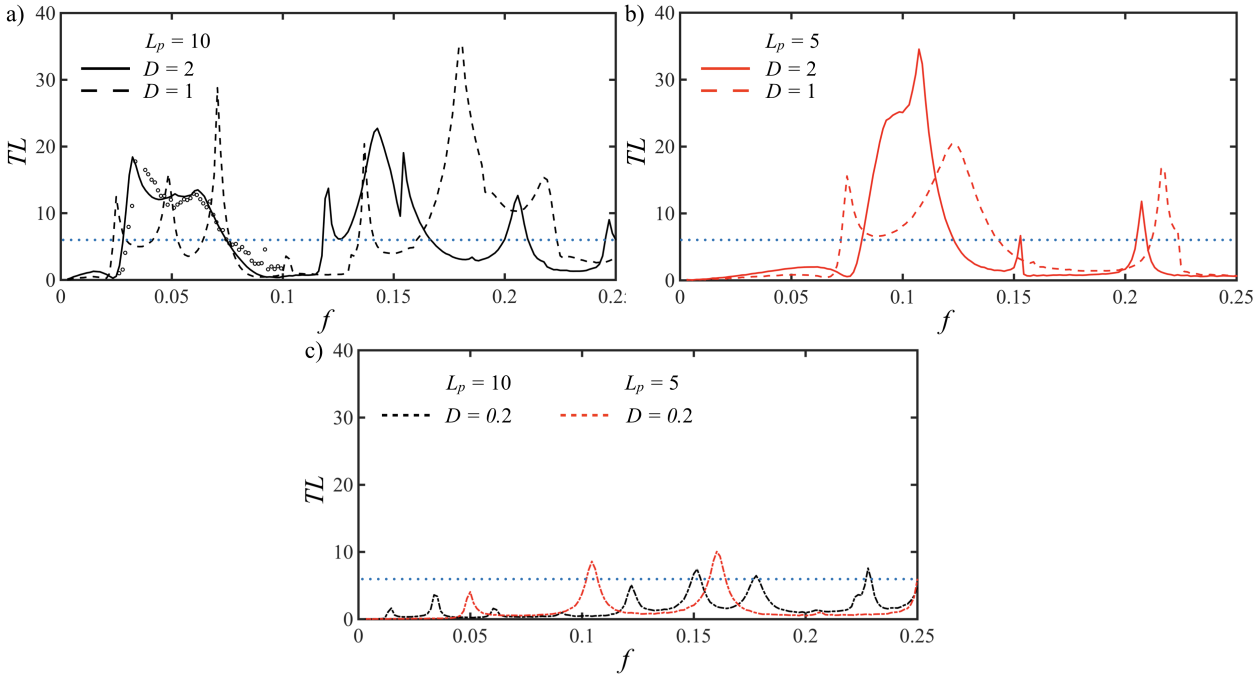

Figure 2: Transmission loss (dB) of EP liner with different cavities. a) $L_p = 10$. Black circles denotes the experimental results [11]. Two erroneous experimental results at $f \sim 0.03$ are omitted and reader are referred to Fan et al.[17] for details; b) $L_p = 5$ and c) $D = 0.2$. Blue dotted lines show 6 dB level.

Fig. 2a, TL for $L_p = 10$ comprises of several alternating plateaus ($TL \geq 6$ dB) and troughs ($TL < 6$ dB) over the excited frequency band. A plateau and a trough in TL correspond to a high transmission band (HTB) and a low transmission band (LTB) respectively. The 6-dB criterion marked by blue dotted line in the figure refers to a reduction of incoming acoustical energy by half and is a convenient choice aiding to describe the acoustic behaviors observed. The maximum attained TL can reach above 30 dB. Similar behavior also occurs at $L_p = 5$ (Fig. 2b) but the patterns of TL shift to high frequency side. The center frequency of first HTB nearly doubles that for $L_p = 10$. The maximum attained TL does not change a lot compared to the panels with $L_p = 10$. For both values of L_p, decreasing the cavity depth D from 2 to 1 shifts the locations of HTB and peaks. Maximum magnitude of TL does not vary much. At some frequencies e.g. $f \sim 0.170$ at $L_p = 10$, TL even increases. However, when the cavity become very thin (T1 and T2), their values of TL for both cases drop significantly which are less than 6 dB in most of the frequency range. This suggests that the cavity depth does plays an role in determining the acoustic behavior of EP liners and different noise mitigation mechanisms may come into play in these thin cavities. The rectangular EP liner configuration are categorized into one with thick cavity (S1, S2, S3 and S4) and another with very thin cavity (T1 and T2) for further analysis.

3.1.1. Thick-cavity EP Liners

The transmission coefficient $\mathscr{T} = \left|p_2^+/p_1^+\right|$, the reflection coefficient $\mathscr{R} = \left|p_1^-/p_1^+\right|$, and the absorption coefficient $\mathscr{A}$ are common representations of overall acoustic behavior [3, 23]. Fig. 3 illustrates $\mathscr{T}$ (blue lines), $\mathscr{R}$ (red lines), and $\mathscr{A}$ (green lines) for different EP liner configurations S1 to S4. Taking the effect of mean grazing flow into account, $\mathscr{A}$ is calculated by the equation [24],

$$\mathscr{A} = 1 - \left(\frac{1 - M_\infty}{1 + M_\infty}\right)^2 \mathscr{R}^2 + \mathscr{T}^2. \tag{4}$$

In a board sense, $\mathscr{A}$ represents all the acoustical energy that are neither transmitted to the upstream nor downstream branches. Since in the present study no structural damping is assumed in panel dynamics, the absorption of EP liner is expected to be associated with the panel vibrations whose energy distributions are also plotted in the figure (magenta dashed lines). The vibration energy is calculated by summing the power of panel vibrating traverse velocity $v_p = \partial\delta/\partial t$ over the panel in their corresponding FFT spectra.

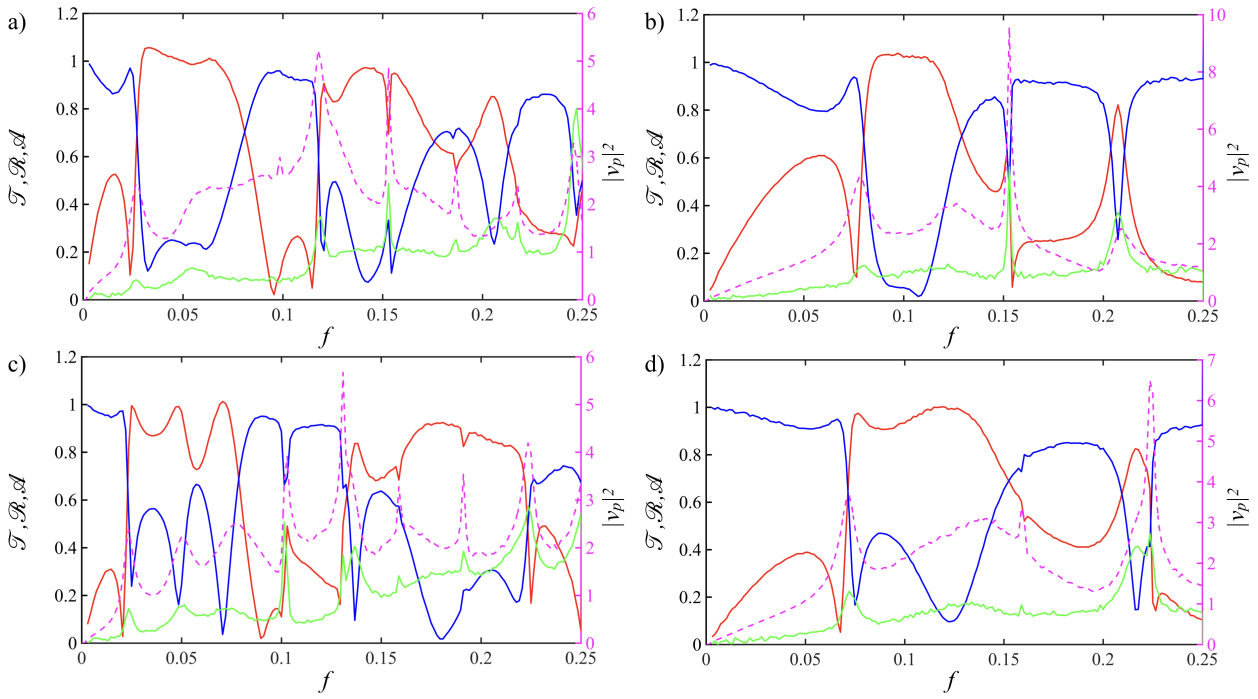

Figure 3: Transmission coefficient $\mathscr{T}$ (blue lines), reflection coefficient $\mathscr{R}$ (red lines), absorption coefficient $\mathscr{A}$ (green lines), and panel vibration energy $|v_p|^2$ (magenta lines) of EPLs with different rectangular cavities. a) case S1 ($L_p = 10, D = 2$); b) case S3 ($L_p = 5, D = 2$); c) case S2 ($L_p = 10, D = 1$); d) case S4 ($L_p = 5, D = 1$).

One should note that $\mathscr{T}$ represents the total amount of propagating acoustic waves downstream from the liner ($x > L_p/2$). The transmitted waves are in fact a mixture of the incident excitation waves and the re-radiated waves generated by vibrating panel. As they have the same frequency and propagating velocity, it is extremely difficult to separate them. Similarly, $\mathscr{R}$ describes the total amount of the acoustic waves propagating upstream from the liner ($x < -L_p/2$) and combines the incident waves reflected at liner boundary and the re-radiation by the panel. These are also indistinguishable due to possessing the same frequency and propagating velocity.

Generally speaking, all $\mathscr{T}$s display broad ranges with values smaller than 0.5 corresponding to a LTB defined with TL. Longer L_p creates more LTBs rather than broadens them. In these LTBs, $\mathscr{R}$ is large (> 0.8) when $\mathscr{T}$ is small. Conversely, large $\mathscr{T}$ is associated with small $\mathscr{R}$ for these panels in the HTBs. The trends of these two coefficients are exactly opposite to each other. In some frequency bands such as $0.160 < f < 0.200$ in S1, both coefficients are larger than 0.5. On the other hand, $\mathscr{A}$s are all very low (< 0.2) and only rise to 0.2 at $f > 0.100$ except some local peaks. The trends of $\mathscr{A}$s agree very well with the panel vibrations in all these cases. All peaks of $\mathscr{A}$ match closely with resonant panel vibrations marked by the peaks of vibration energy. These observations clearly reveal that the panel vibration is a major element of the absorption mechanism in EP liner. Furthermore, all local peaks in these coefficients do not overlap with the natural frequency (Table 2) demonstrating the effect of grazing flow on the acoustic behaviors of EP liner. Based on the present results, the troughs of $\mathscr{T}$, i.e. TL peaks, obviously overlap with the peaks of $\mathscr{R}$ rather than resonant panel vibrations, in contrast to the literature [4, 9, 11, 10]. Those works claimed that the TL peaks were the direct consequences of resonant panel vibrations, i.e. peaks of $\mathscr{A}$. The inaccurate claim may be due to their application of modal analysis, which cast the panel vibrations into *in vacuo* modes. In fact, the panel vibrations are composed of opposite propagating flexural waves which may not synchronize to form *in vacuo* modes in the presence of grazing flow. They also assumed an in-phase relationship between these modes. These all leads to the inaccuracy in the association with TL peaks to resonant panel vibration. The variations of all three coefficients indicates that after excitation, the liners radiate acoustic waves to the duct again rather than absorb the acoustical energy. Otherwise, the absorption should be rather high at frequencies with small $\mathscr{T}$ in LTB. Therefore, the noise mitigation of EP liner is mostly attributed to the wave canceling in which the re-radiated waves by the panel interfere in a destructive manner with the

incident waves reaching downstream from liner.

The absorption of acoustical energy seems to play a minor role in noise mitigation over most of the interested frequency range. Though the acoustical energy appears lost for sustaining resonant panel vibration, the absorption in all these cases is not merely a result of energy dissipation via structural damping because it is neglected in the present formulation. Similar observations are also found in the frequency domain numerical results of Choy and Huang [11] which also ignored such damping and agreed very well with their own experimental results (Fig. 2). This hints that the involvement of additional noise mitigation mechanism. Since the panel radiates acoustics again to the duct and cavity after excitation, the major acoustic absorption should occur in fluid rather than in panel [25]. We will explore the mechanism of such absorption later.

Comparing the variation with D, similar trends of the coefficients are observed for both values of L_p, but a shallower cavity tends to create more wriggles in these coefficients and shift the frequencies of resonant panel vibration. It probably connects with the change of cavity impedance due to air compressibility when D decreases. The impedance can be expressed as $Z_C = 1/i \tan(kD)$ where k is the wave number [23]. Since this impedance manifests a periodicity due to the tangent function, decreasing the depth shortens the period of changing in Z_C and leads to quick changes in the acoustic coefficients over frequency.

As the incident acoustic excitation mixes well in the flow duct with the reflected, the transmitted and the re-radiated waves from the panel, it is difficult to reveal the response of the liner to the incident excitation. Therefore, a procedure is employed to estimate the response and its subsequent effect on eventual acoustic propagation upstream and downstream of liner. For each case a fully rigid duct of same dimensions is built and propagation of same acoustic excitation through same grazing flow inside rigid duct is calculated in temporally synchronized manner as the duct with liner. The acoustic solution with rigid duct, hereafter referred as incident acoustics p_1^+, is then subtracted from the total solution p' with liner to obtain the re-radiation p'_R contributed by the liner, i.e. $p'_R = p' - p_1^+$. A comparison of the phase between the re-radiation and incident acoustics may shed light on the mechanism responsible for the transmission characteristics of observed downstream of liner. Fig. 4 illustrates the distribution of the magnitude of phase, normalized by π, between incident acoustics and re-radiated wave along the quarter-line (i.e. $y = H/2$) of duct computational domain. The phases are determined from cross spectra of the solutions $S_{I,R}(f) = \sum_{m=-\infty}^{\infty} R_{I,R}(m)\, e^{-i2\pi f m}$, where $R_{I,R}$ is the cross-correlation between p_1^+ and p'_R in each case. Several observations can be made from

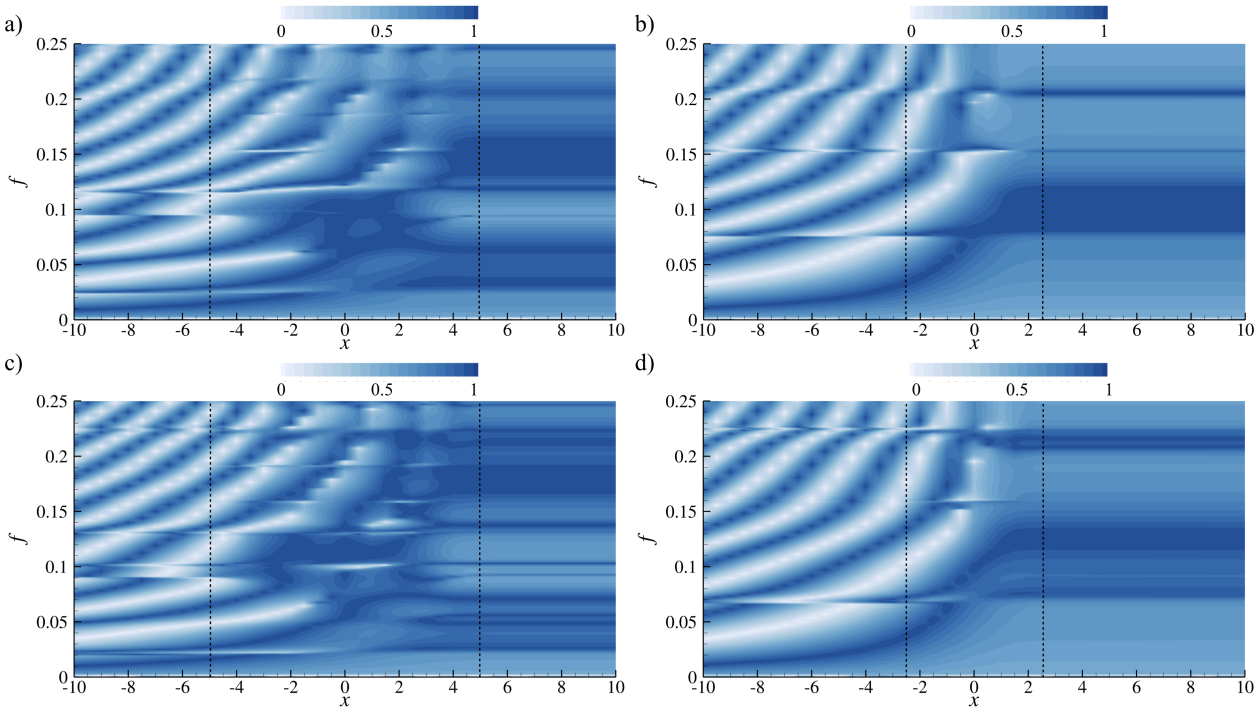

Figure 4: Absolute phase distribution (normalized by π) of cross spectra between incident waves and re-radiated acoustic pressure along duct centerline. Regions between dashed lines are the liner regions. a) case S1 ($L_p = 10, D = 2$); b) case S3 ($L_p = 5, D = 2$); c) case S2 ($L_p = 10, D = 1$); d) case S4 ($L_p = 5, D = 1$).

this figure. Firstly, in each case a specific curved strip pattern is observed in region covering the upstream branch of the duct. The pattern is characteristic for the overlapping of two opposite propagating waves i.e. the incident acoustics and the reflected waves. The periodicity of stripe pattern along x is roughly half wavelength of the incident acoustics so the separation of the stripes becomes narrower at high frequencies. Secondly, the curved stripe pattern appears to originate deeply from liner region ($-L_p/2 \leq x \leq L_p/2$). This implies that the reflected acoustic waves are in fact the re-radiation generated by the vibrating panel under excitation by the incident acoustics. Thirdly, a horizontal strip pattern of constant phase along x is observed downstream of the liner in each case. The pattern can be considered as a result of overlapping of incident acoustics and transmitted acoustic waves propagating in same direction. The extent of interference of these two waves is observed to vary with excitation frequency. In particular, the deep blue regions appear to overlap with LTBs (with high TL) because the incident acoustics and transmitted acoustic wave constitute a very effective destructive interference due to their almost out-of-phase relationship. Similarly, the light blue regions overlap with HTBs (with low TL) as a consequence of limited constructive or even destructive interference due to very little phase between the incident acoustics and transmitted acoustic wave. It is interesting to note that all the horizontal strip patterns of constant phase begin insider liner region. This implies that the interference is complete before the acoustics leaves the liner.

The vibratory responses of the panels are examined in order to gain further understanding of elastic panel liner mechanism. Fig. 5 shows the dispersion relations of flexural wave propagations in cases S1 and S2. The theoretical relation is obtained by using the method derived for panel of infinite length [6] and is denoted by solid lines. To deduce the dispersion relation from the numerical results, two-dimensional FFTs are performed on panel vibrating velocity v_p and then the local peaks for each frequency are selected as they represent the actual panel vibrations in the cases. The resolution in wave number k depends on length of the panels originally, but both panels are much shorter than the required length for sufficient resolution in k. Therefore, zeros are padded in the spatial direction for 10 times of original data length to increase the resolution in k. It however also increases the aliasing error in the spectra. Because of the overwhelming of this error, the dispersion relations from the two-dimensional FFTs for $L_p = 5$ are not reliable so they are omitted here. In theory, the dispersion relation of elastic panel depends on the material properties of the panel only. It possesses a subsonic branch (black line) and supersonic branch (blue line) based on comparison

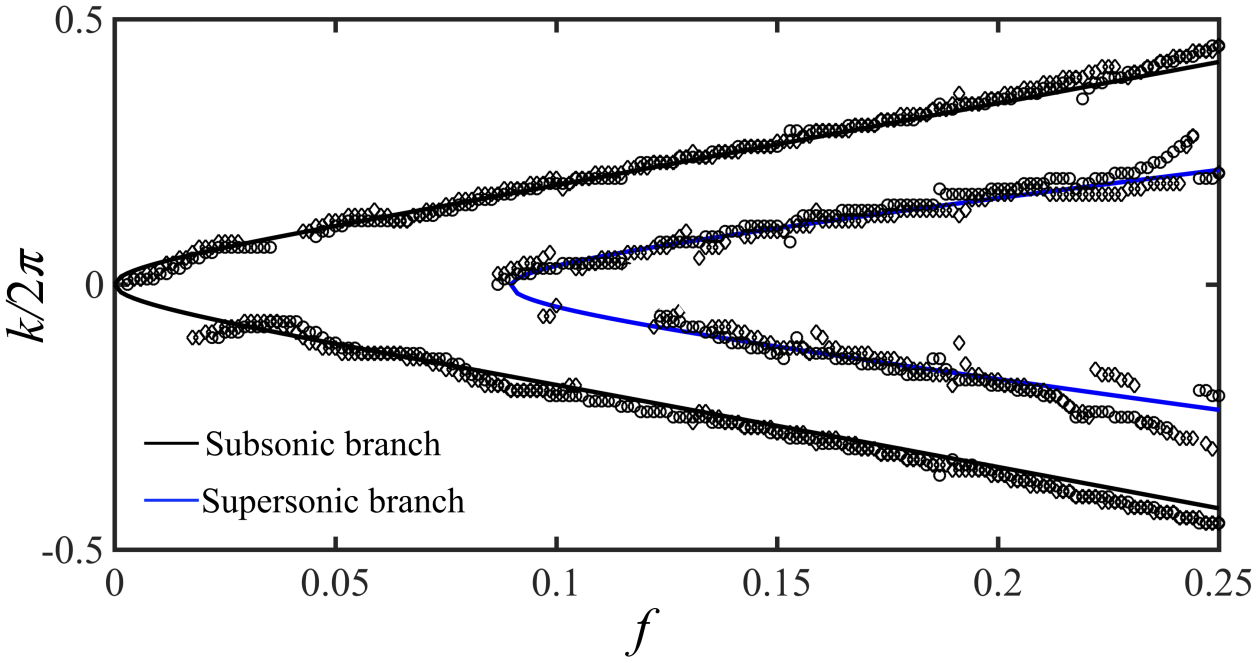

Figure 5: Dispersion relationship of elastic panels. Black circle: case S1 ($L_p = 10, D = 2$); Black diamond: case S2 ($L_p = 10, D = 1$).

of flexural wave propagating speed with the ambient acoustic speed in fluid. For the present panels, the supersonic branch exists only beyond critical frequency $f_{cr} = 0.090$ that is independent of panel length. The calculated relations in these panels generally agree well with the theoretical results. Cavity depth does not influence the flexural wave speed in these cases. Comparing to the absorption shown in Fig. 3, $\mathscr{A}$ shows an gentle increase at $f \geq f_{cr}$ and shows more resonant panel vibration than those at $f < f_{cr}$. This may be due to the existence of supersonic flexural waves that increases the opportunity of creating resonant panel vibration. In addition, the existence of the supersonic branch also creates more changes in the transmission behavior of EP liner (Fig. 3).

Figure 6 depicts the magnitudes of cross power spectral densities between the incident acoustic pressure p'_C at probe C $(x, y) = (-L_p/2, 0.5)$ in Fig. 1 and the vibrating velocity v_p of the panels in cases S1 - S4. The cross power spectral density is defined as

$$S_{C,v_p}(f) = \sum_{m=-\infty}^{\infty} R_{C,v_p}(m)\, e^{-i2\pi f m}, \tag{5}$$

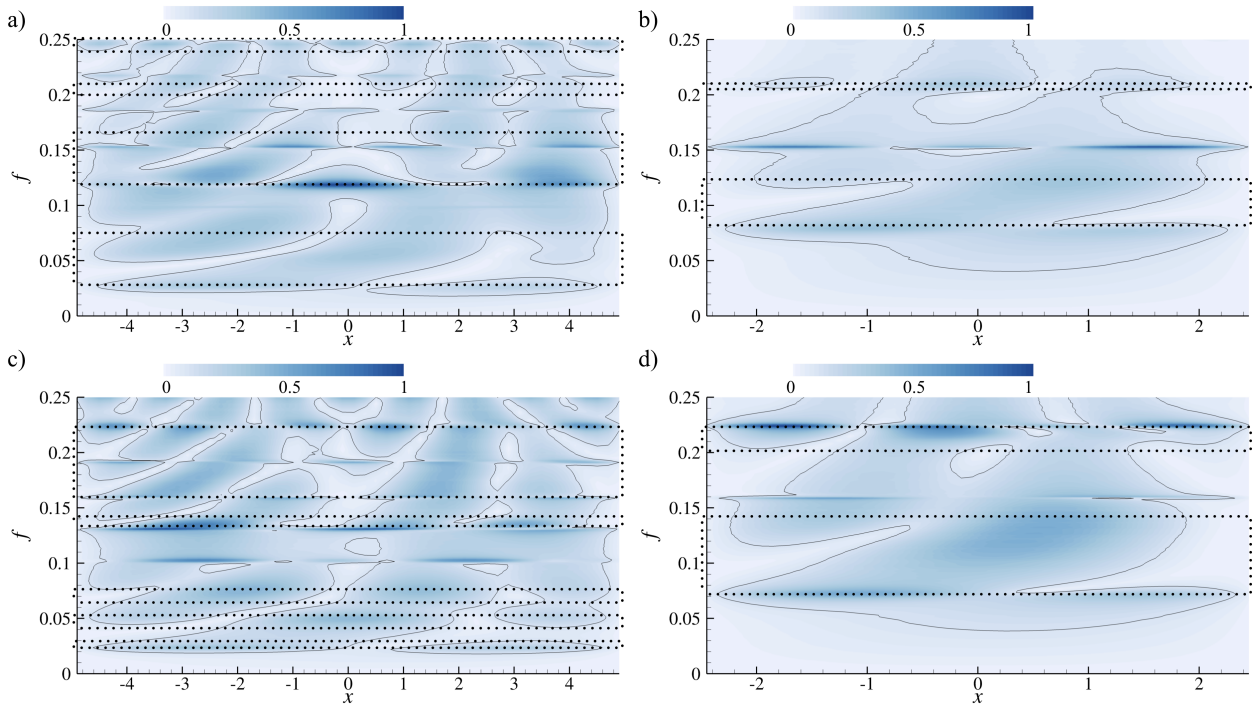

Figure 6: Normalized magnitude of cross power spectral density between p'_C at probe C and v_p of elastic panels. a) case S1 ($L_p = 10, D = 2$); b) case S3 ($L_p = 5, D = 2$); c) case S2 ($L_p = 10, D = 1$); d) case S4 ($L_p = 5, D = 1$).

where R_{C,v_p} is the cross-correlation between p'_C and v_p in each case. It is calculated by using the Welch method with sampling frequency $f_s = 20$ and 50% of data overlapping and is normalized by the maximum magnitude in the case. The contours in the figure mark 10% of respective maximum magnitudes in all cases, which represent regions with very small response. Dotted rectangles mark all the LTBs determined from Fig. 3. Large values in the figure correspond to large and either in phase or out of phase response from panel. Small values indicates either little panel responses. All the values near the ends of panels are very low due to the constraints of simply supported boundary conditions. Across the panels, the cross spectra possess alternating regions of peaks and troughs in all frequencies. These characteristics shift to right and becomes narrower with increasing frequency. Number of such repeating patterns also increases as f increases, but there are no obvious trends observed for the LTBs and HTBs. Referring to Fig. 3, the panel responses at peaks of absorption are always very high in some panel regions, e.g. $-1 < x < 1$ at $f \sim 0.120$ in case S1 (Fig. 6a). Nevertheless, these high levels of panel response do not guarantee a large noise mitigation such as at $f \sim 0.224$ in case S3. In some LTBs, the cross spectra also show quite high values outside the resonant panel vibration, e.g. $x > 1$ at $f \sim 0.120$ in case S4 (Fig. 6d).

The phases ϕ_{C,v_p} of S_{C,v_p} are unwrapped [26] and are normalized with π for ease of interpretation (Fig. 7). Dotted rectangles mark all the LTBs determined from Fig. 3. Considering Fig. 3 and Fig. 7 together, several panel behaviors related to incident acoustics are observed. In general, the variations in ϕ_{C,v_p} across panel at $f < f_{cr}$ are much simpler than those at $f \geq f_{cr}$. The panel vibration depends very much on the existence of supersonic branch in flexural wave propagation at $f \geq f_{cr}$. At $f < f_{cr}$, ϕ_{C,v_p} varies gradually across the panel in HTB. As two flexural waves propagating in opposite directions on panel in non-synchronized manner, different locations of panel vibrate at their own phases with respect to the incident acoustics leading to variation in ϕ_{C,v_p} across the panel. In the the frequency band with high $\mathscr{R}$ (LTB), fairly horizontal contours dominate on different portions of panel which are separated by abrupt changes in ϕ_{C,v_p}. The horizontal contours indicate constant phase which means that portions of panel in these regions vibrate altogether more or less in a synchronized manner with incident acoustics. Such vibration most likely constitutes a standing flexural wave on panel. According to Fig. 3, the panel standing wave produces an effective re-radiation which propagates into both upstream and downstream directions. Strong upstream re-radiation leads to high $\mathscr{R}$ while its downstream counterpart most likely creates effective

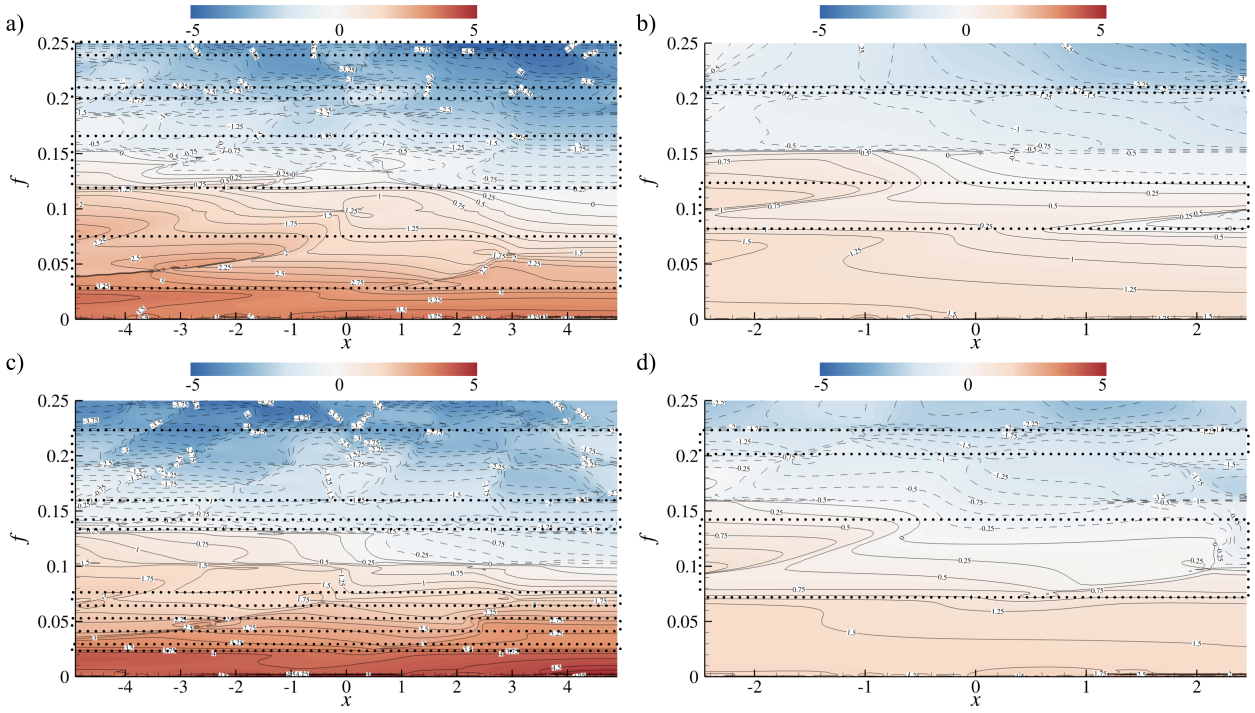

Figure 7: Normalized phase ϕ_{C,v_p} between p'_C at probe C and v_p of elastic panels. a) case S1 ($L_p = 10, D = 2$); b) case S3 ($L_p = 5, D = 2$); c) case S2 ($L_p = 10, D = 1$); d) case S4 ($L_p = 5, D = 1$).

destructive interference with the incident acoustics leading to low $\mathscr{T}$. However, there is no specific phase relationship between the incident acoustics and the panel vibration observed in regions with high values of $\mathscr{T}$ and $\mathscr{R}$. The phase also becomes increasingly complicated at $f \geq f_{cr}$. There exists some frequency bands with quite large $\mathscr{T}$ and $\mathscr{R}$ (> 0.5), in which complicated phase patterns occurs. One of the example is at $0.170 < f < 0.190$ in case S1. Gradual change and horizontal contours with abrupt change are at $x < 0$ and $0.5 < x < 5$ respectively. This is due to the fact that supersonic and subsonic flexural waves with different speeds re-radiate different acoustic waves to the duct, creating different types of interference at upstream and downstream of the liner. This is not observed in $f < f_{cr}$, in which only subsonic flexural waves propagate in the $+/-$ x-axis. In addition, resonant panel vibration seems connected to a sudden change in ϕ_{C,v_p} across frequency as indicated by clustered contours across whole panel near frequency. An obvious example is the resonant panel vibration at $f \sim 0.152$ in case S2. This is similar to the phase change found near resonance in structural dynamics. Finally, the effect of D can be observed by comparing the sub-figures vertically. Small effect of D on ϕ_{C,v_p} are observed. ϕ_{C,v_p} overall demonstrates similar distribution in both panel lengths except some frequency shifts of the resonant panel vibrations.

Since the transmission behavior of EP liner depends very much on whether the vibration is within supersonic branch, it is simpler to inspect the acoustic behavior at $f < f_{cr}$ for unveiling noise mitigation mechanism. However, the fundamental mechanism should also work in the same manner at $f \geq f_{cr}$. Some peaks of $\mathscr{T}$, $\mathscr{R}$ and $\mathscr{A}$ in case S4 at $f < f_{cr}$ are chosen to illustrate the general acoustic phenomenon in the HTB and LTB. Fig. 8 shows an example with $\mathscr{T} \sim 1$ at $f = 0.066$ in case S4 ($L_p = 5$ and $D = 1$). At this frequency, the wavelength is longer than the panels such that the panel does not experience a whole wavelength. Only subsonic branch of flexural waves exist on the panel. In this figure, snapshots of acoustic pressure p' and δ distributions (black lines at cavity) are plotted with a time increment of one eighth of its period. The distributions of δ are exaggerated but are in the same scale among all sub-figures. One should note that all similar snapshots in forthcoming discussions are prepared in the same way. In this case, opposite propagating flexural waves are observed on the panel. The acoustics inside cavity also propagates with opposite directions in a nearly plane wave pattern. Both the flexural waves and acoustics inside cavity are however not synchronized to form standing wave pattern. This is consistent with the observed gradual change of ϕ_{C,v_p} across the panel in HTB. They seem to have little effects on the acoustics inside the duct.

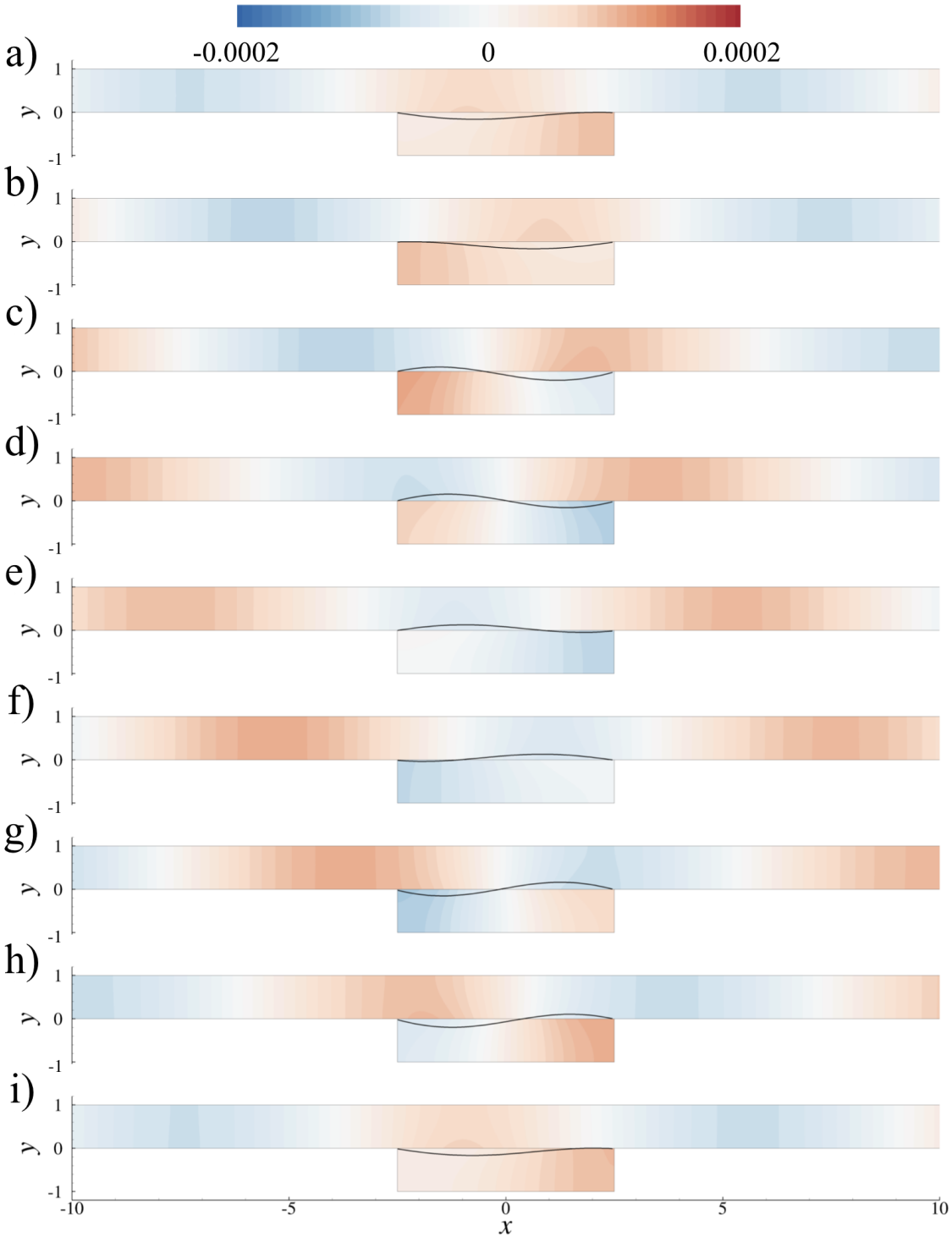

Figure 8: Snapshots of p' and δ distributions (black lines) at $f = 0.066$ ($\mathscr{T} \sim 1$) in case S4.

The duct acoustic waves appear to just pass over the liner without obvious changes; p' slows down slightly in the liner region and changes slightly near the elastic panel leading to non-planar contours. The re-radiated waves are in fact very weak as indicated by the small $\mathscr{R} \sim 0$ at this frequency. Even when $\mathscr{R}$ is a bit larger at frequency in HTB, the re-radiated waves may be almost in phase with the incident acoustics causing little noise mitigation in HTB.

As an illustration with LTB, Fig. 9 shows the snapshots of p' and δ distributions (black lines at cavity) at $f = 0.077$ ($\mathscr{R} = 1$) in case S4. The acoustic pressure inside cavity and the flexural waves oscillate in standing wave patterns. A slant acoustic nodal line inside cavity resides at $x \sim 0.1$ near the panel. On the panel, the node of flexural wave is observed at $x \sim 0.5$ which corresponds to a region with abrupt change in ϕ_{C,v_p} (Fig. 7d). This standing wave oscillation of panel creates the horizontal contours and the regions with abrupt change across panel found in ϕ_{C,v_p} (Fig. 7) inside LTB. The latter are indeed nodes of these standing wave patterns. The slant nodal line in cavity also shows that the plane wave assumption inside the cavity in the literature is not accurate. In addition, non-planar waves are also observed near the panel inside the duct e.g. at origin in Fig. 9d. This illustrates the high order mode re-radiation by the panel whose downstream radiation interferes destructively with the incident acoustics in the downstream branch of the liner. This leads to noise mitigation in transmitted wave.

Fig. 10 demonstrates the instantaneous distributions of p' and δ at a local absorption peak in case S4 ($f = 0.072$). At this frequency, the panel vibrates in the most vigorous manner among the cases of different peaks in $\mathscr{T}$ and $\mathscr{R}$. It vibrates in a pattern quite similar to standing wave but its node jitters continuously on the panel within a range of $0.1L_p$ on the panel. The acoustics inside cavity also behaves in a similar way. The re-radiation creates an standing wave oscillation of acoustic pressure with nodal jittering in upstream branch and a continual transmission through downstream branch to duct exit. The panel vibrations are indeed very similar to those observed in the case with large $\mathscr{R}$. Their difference in $\mathscr{A}$ may be associated with the acoustic re-radiation by the panel because as aforementioned the acoustic energy should be lost to the fluid rather than via the structural damping in these cases. Inspecting the vicinity of the panel carefully, the instantaneous distribution of p' exhibits several semi-circular contours along the panel. Since the ends of panels are simply supported, its acoustic radiation shows similarity to that of a wave guide such that it radiates in plane wave mode and other high order modes [27]. Therefore, upon excitation the panels radiate

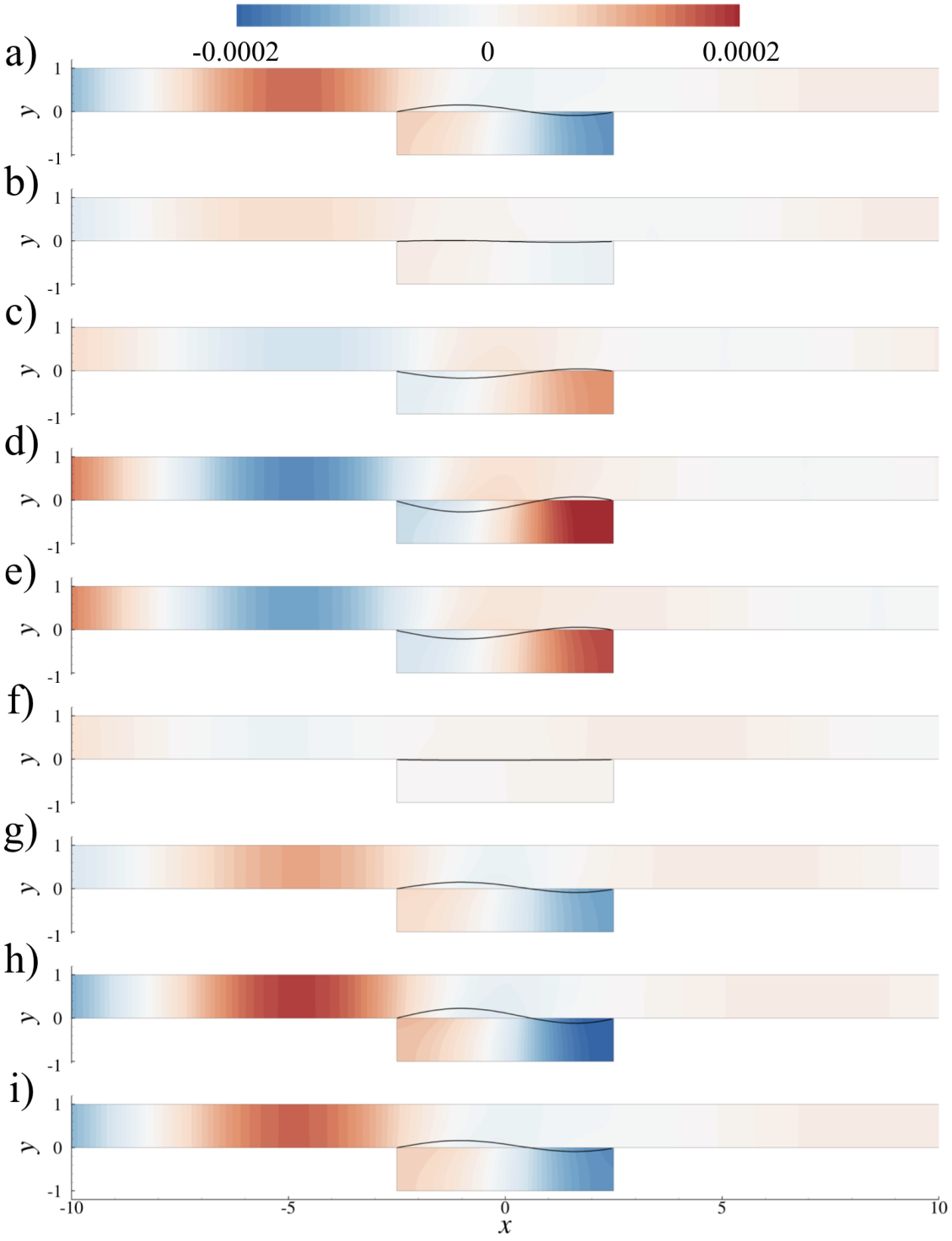

Figure 9: Snapshots of p' and δ distributions (black lines) at $f = 0.077$ ($\mathscr{R} \sim 1$) in case S4.

the acoustics in all these modes to the duct and the cavity. However, as the frequency of radiation is smaller than duct cut-off frequency ($f_{cutoff} = 0.500$), only plane wave mode can propagate along the duct but the high order modes attenuates exponentially. As such, the energy used in exciting high order modes is lost in the upstream and downstream branches. When the frequency of incident acoustics matches that of resonant panel vibration, the panel vibrates vigorously by tapping a lot of incoming acoustical energy leading to an increase in energy loss via high order mode acoustic radiation. Actually high order mode radiation at other frequencies also occurs near the panel, but they are not very clear e.g. the semi-circular contours near $x \sim 1$ in Fig. 8b and origin in Fig. 9d. This also explains the increasing trends of $\mathscr{A}$ with frequency as it is relatively easy to create high order mode in decreasing wavelength. One should note that this mechanism here is not the dominant mechanism of noise mitigation at this local absorption peak. Strong reflected and transmitted waves are observed. This is confirmed by a relatively large $\mathscr{T}$ and $\mathscr{R}$ (> 0.5) as shown in Fig. 3d. The only observed case in which this mechanism becomes essential is the absorption peak at $f \sim 0.245$ in case S1. Both $\mathscr{T}$ and $\mathscr{R}$ are quite low (~ 0.3). This means that panel does not radiate much acoustics of plane wave mode to the duct. As f further increases (> 0.200), the acoustics pressure in the upstream branch oscillates in a pattern similar to that at $f = 0.072$ while that oscillates at irregular pattern inside cavity and has large variation along cavity depth (Fig. 11).

3.1.2. Shallow-cavity EP Liners

Fig. 12 shows $\mathscr{T}$, $\mathscr{R}$ and $\mathscr{A}$ together with the vibration energy of panel for cases T1 and T2. Generally speaking, $\mathscr{T}$ is much higher than liners with thick cavity (cases S1 - S4). This is consistent with the low TL shown in Fig. 2c. The panel responses are also weaker than liners with thick cavity except at the resonant panel vibration. This leads to weaker re-radiation by panels as indicated by small $\mathscr{R}$. The trends of $\mathscr{T}$s are still opposite to those of $\mathscr{R}$s. Unlike the reported observations with thick cavity, the trends of $\mathscr{R}$s essentially follow those of $\mathscr{A}$s and vibration energy of panels. In these shallow-cavity liner, the troughs in $\mathscr{T}$ are in close alignment with the peaks of $\mathscr{A}$, panel vibration energy and $\mathscr{R}$. The panel appears set into resonant vibration and its re-radiation, then interferes with the incident acoustics destructively in the downstream branch. Thus, the dominant mechanism of noise mitigation is still wave canceling. The absorption via high mode acoustic radiation is only dominant at the resonant panel vibration at $f = 0.225$ in case T1 in which

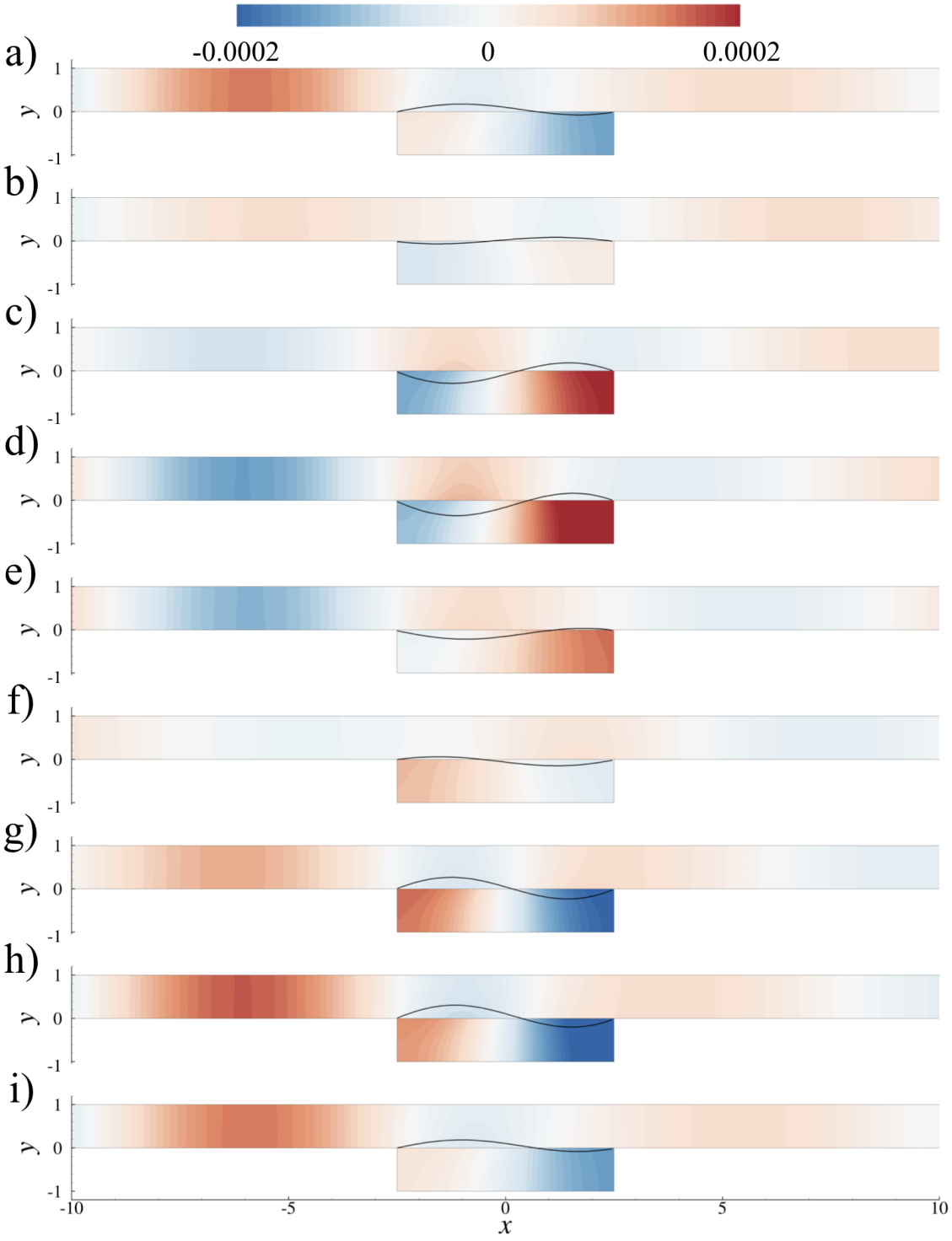

Figure 10: Snapshots of p' and δ distributions (black lines) at $f = 0.072$ (Local peak of absorption) in case S4.

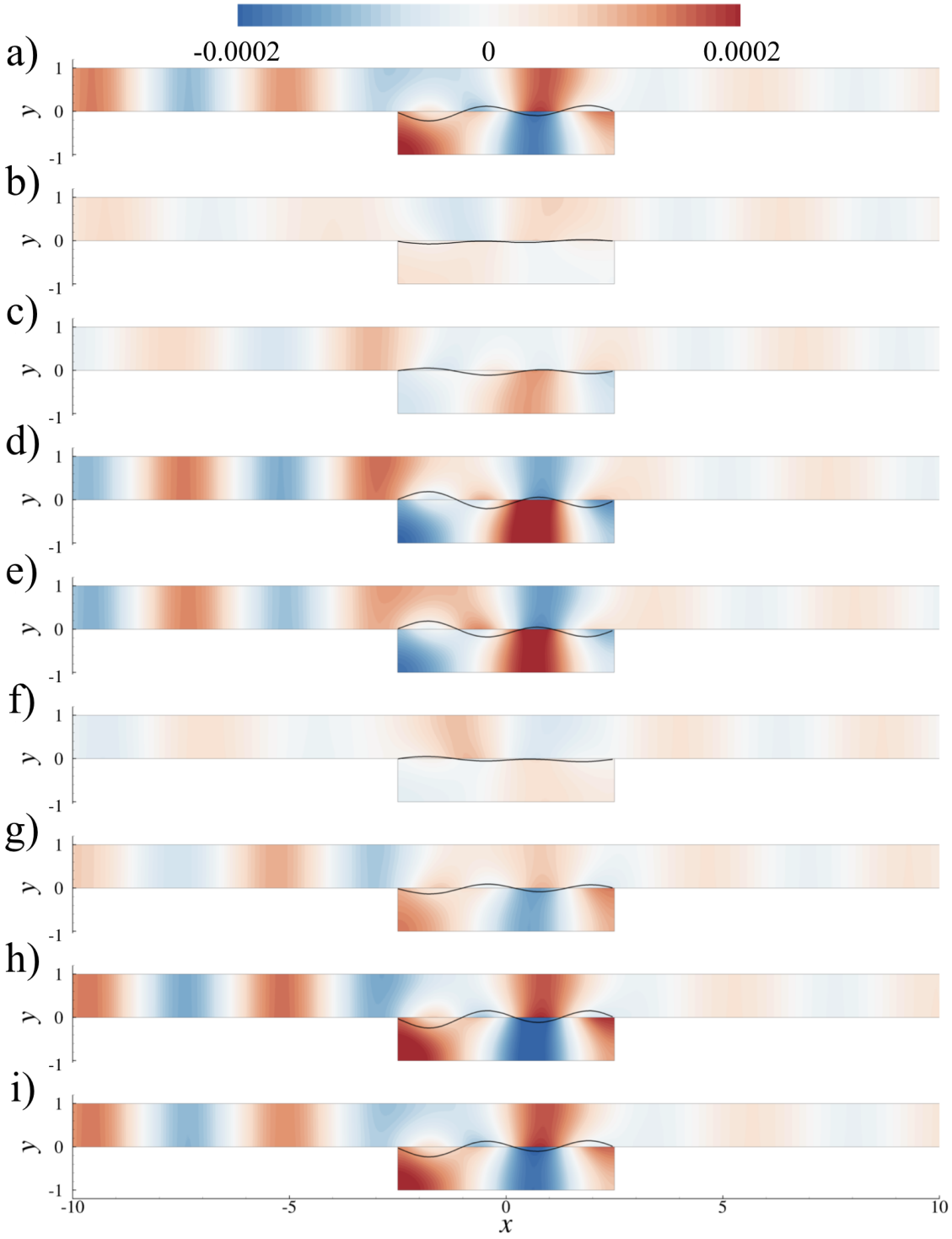

Figure 11: Snapshots of p' and δ distributions (black lines) at $f = 0.223$ (Local peak of absorption) in case S4.

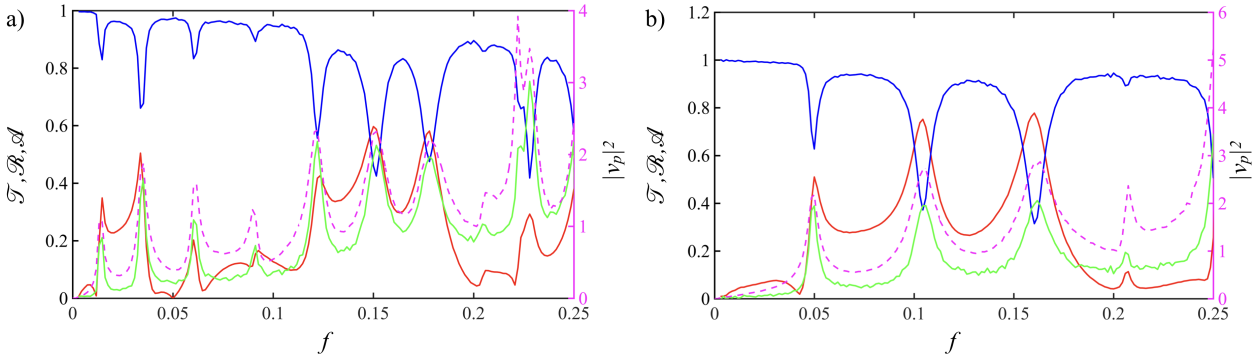

Figure 12: Transmission coefficient $\mathscr{T}$ (blue lines), reflection coefficient $\mathscr{R}$ (red lines), absorption coefficient $\mathscr{A}$ (green lines), and panel vibration energy $|v_p|^2$ (magenta lines) of EPLs with different cavities a) case T1 ($L_p = 10$, $D = 0.2$); b) case T2 ($L_p = 5$, $D = 0.2$).

$\mathscr{T}$ (~ 0.4) and $\mathscr{R}$ (< 0.3) are rather weak. In addition, the reduction at resonance frequency $f < 0.100$ is improved when the panel length is reduced from 10 to 5. It is surprised to see that the panel with $L_p = 5$ performs better than that with $L_p = 10$ does at such low frequency.

Fig. 13 shows the dispersion relation of the panel in case T1 only as that in case T2 is contaminated by the aliasing error when performing two dimensional FFT. The wave speed in case T1 is slightly lower than the theoretical values for the subsonic branch. Nevertheless, the critical frequency f_{cr} is shifted to approximately 0.200. It indicates the effect on flexural wave is significant when the panel is in very close proximity of cavity bottom wall. In low frequency range $Dk \ll 1$, the impedance of the cavity can be approximated by $Z_C = 1/ikD$ [23]. Based on the theoretical model [6] and after some arrangements, the dimensionless characteristic equations of panel without damping is

$$\rho_p \frac{\sqrt{\sigma_p/\rho_p}}{c} k^2 - \rho_p (2\pi f)^2 = -i \frac{Z_C}{c} (2\pi f) \approx \frac{1}{Dc}, \tag{6}$$

where k is the wave number of panel vibration. This hyperbolic equation suggests that a reduction in D increases f_{cr} of the supersonic branch.

Figure 14 depicts normalized magnitudes of cross power spectral densities between the acoustic pressure p' at probe C and the vibrating velocity v_p of the panels in cases T1 and T2. In both configurations, the cross spectra show strong resonant panel responses, but their responses at other frequencies are rather weak.

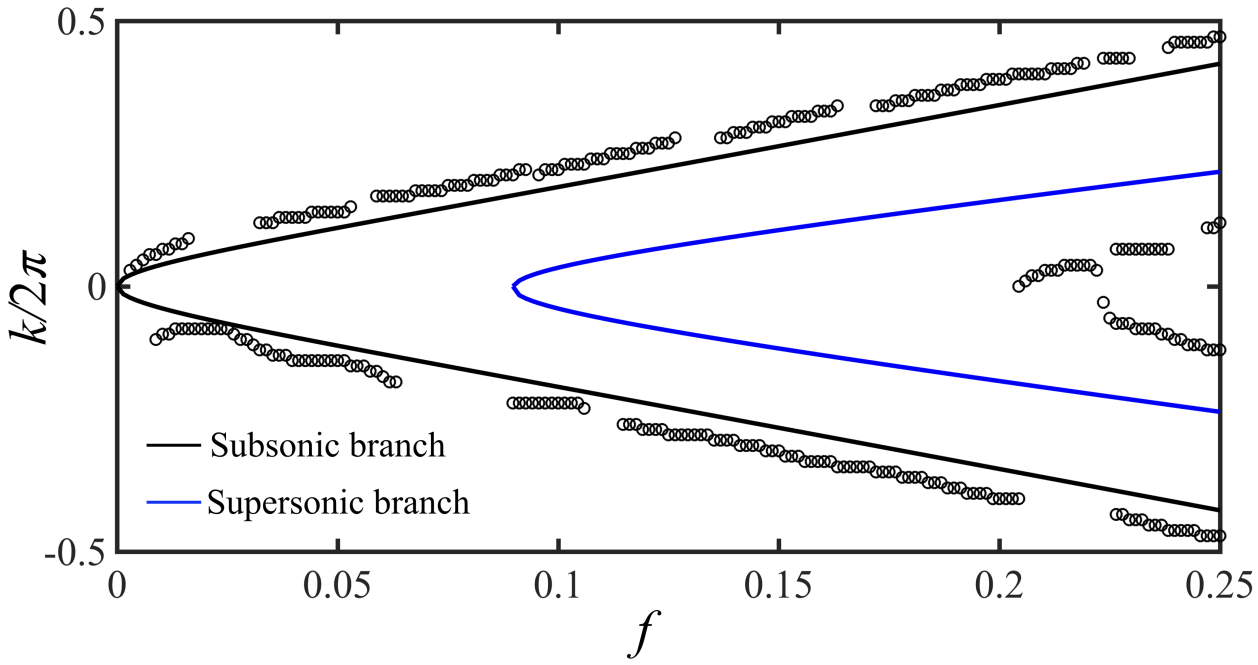

Figure 13: Dispersion relationship of elastic panels in case T1.

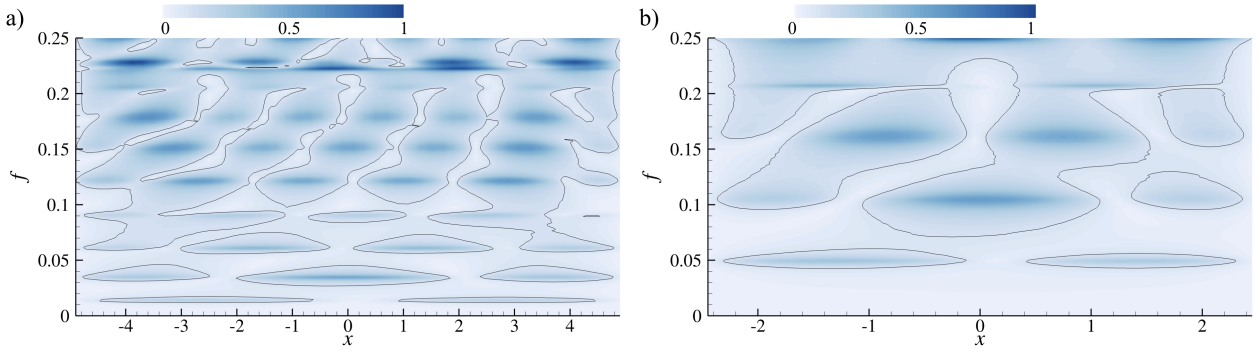

Figure 14: Normalized magnitude of cross power spectral density between p' at probe C and v_p of elastic panels. a) case T1 ($L_p = 10, D = 0.2$); b) case T2 ($L_p = 5, D = 0.2$).

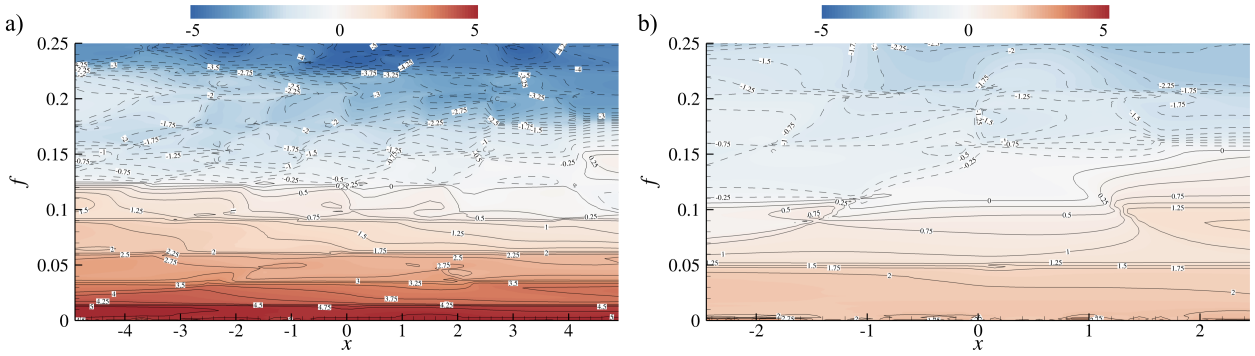

Figure 15: Phase difference between location at probe C and v_p of elastic panels with $L_p/D \geq 25$. a) case T1 ($L_p = 10, D = 0.2$); b) case T2 ($L_p = 5, D = 0.2$).

This observation is in contrast with thick cavity in which the responses of panels are strong even they are not at resonance. The phase ϕ_{C,v_p} of these cross spectra are illustrated in Fig. 15. Similar to previous thick cavity cases, the peaks of $\mathscr{A}$ at frequencies of resonant panel vibration are associated with a sudden phase change across the frequency. Unlike those cases, ϕ_{C,v_p} changes gradually for all frequencies other than the frequencies of resonant panel vibration. This is consistent with the previous observation that gradual changes in ϕ_{C,v_p} across panel connect with large $\mathscr{T}$. Clustered horizontal contours in ϕ_{C,v_p} across panel are only observed near resonant panel vibration which is also consistent with those observed near peaks of $\mathscr{A}$ in thick cavity EP liner.

Since HTB almost covers the entire frequency range, it is worthy of studying a local absorption peak to demonstrate noise mitigation mechanism in shallow cavity EP liner. Fig. 16 demonstrates an example at local absorption peaks at $f = 0.106$ in case T2 using snapshots of its instantaneous p' and δ (black solid lines). Inside the cavity, p' are essentially uniform across the cavity depth and oscillates in standing wave patterns together with the panel. This generates reflected waves and downstream propagating waves which interfere with incident acoustics destructively in downstream branch. High order modes of acoustic radiation are also observed clearly near the panel which decays rapidly inside the duct. Based on this results, resonant panel vibration that initiates both wave canceling and radiations of high order modes is the dominant cause of the noise mitigation in shallow cavity liner.

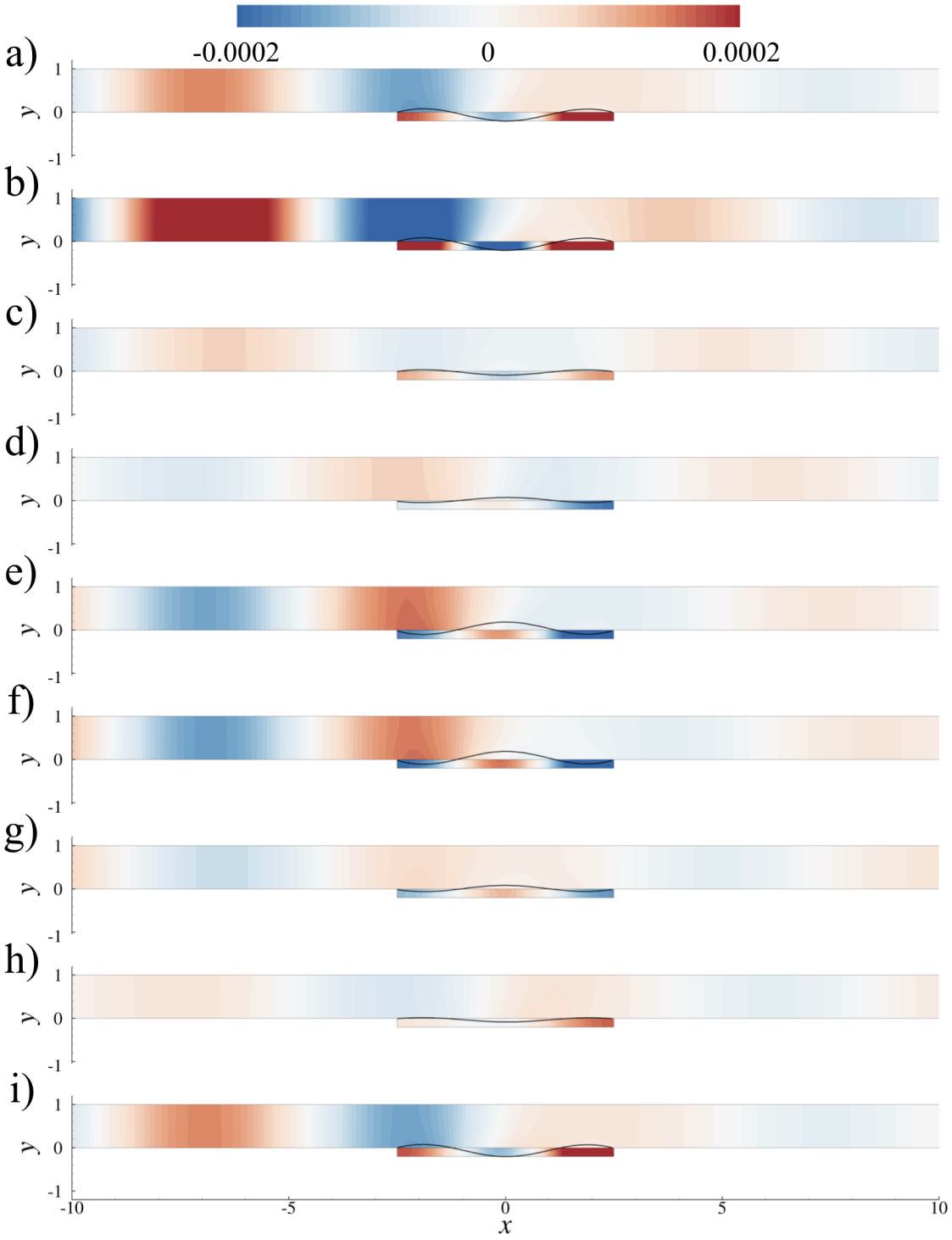

Figure 16: Snapshots of p' and δ distributions (black lines) at $f = 0.106$ (Local peak of absorption) in case T2.

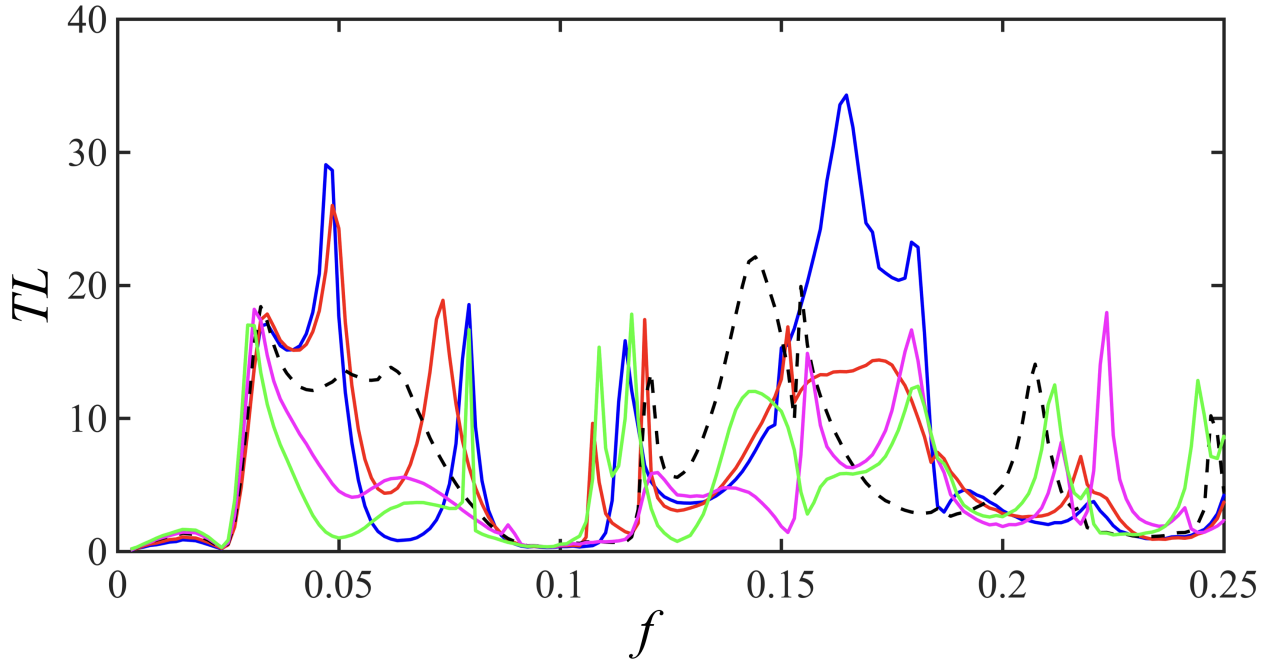

Figure 17: Transmission loss of EP liner with different cavities. Blue line: case C1; red line: case C2; magenta line: case C3; green line: case C4; and black dashed line: case S1

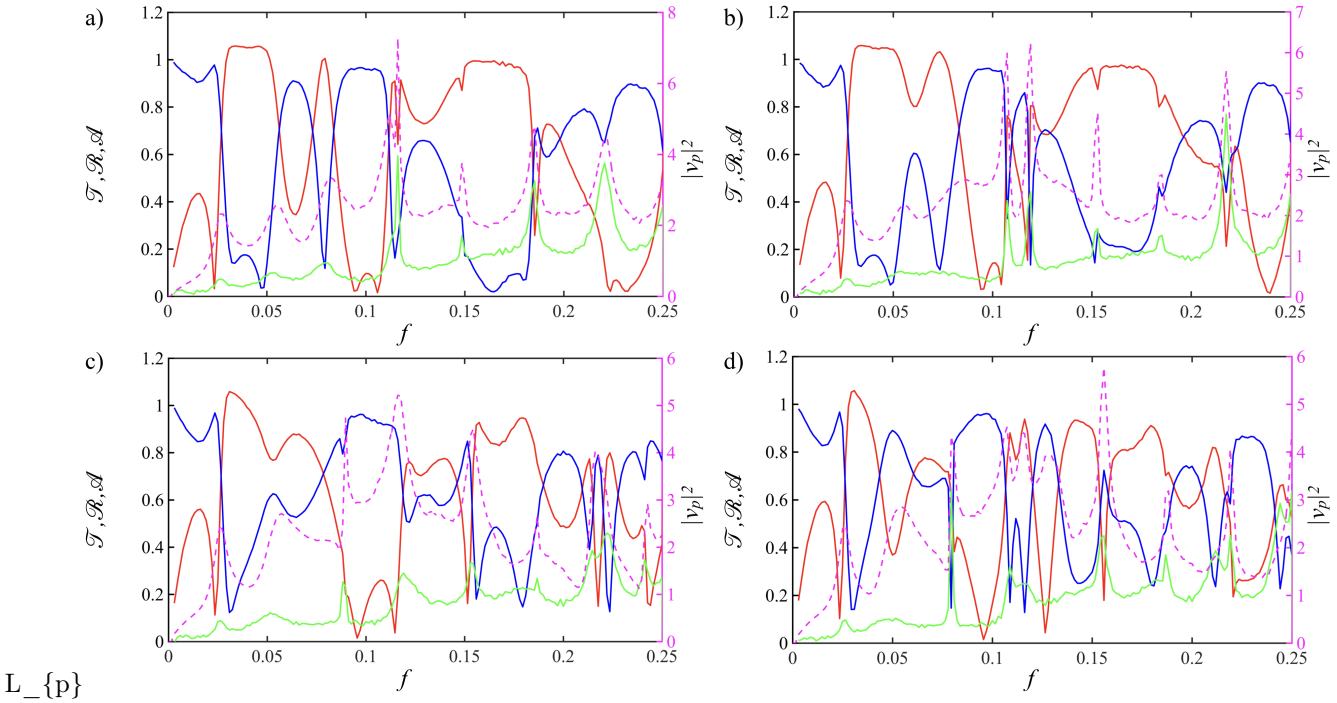

Figure 18: Transmission coefficient $\mathscr{T}$ (blue lines), reflection coefficient $\mathscr{R}$ (red lines), absorption coefficient $\mathscr{A}$ (green lines), and panel vibration energy $|v_p|^2$ (magenta lines) of EPLs with different cavities. a) case C1 ($L_B = 5$); b) case C2 ($L_B = 7.5$); c) case C3 ($L_B = 12.5$); d) case C4 ($L_B = 15$).

3.2. Non-rectangular Cavity

In this section, the results of cases C1 to C4 are examined with case S1 taken as the reference for comparison. The variation among these cases is just the length of the cavity base L_B. Fig. 17 shows TL in these cases. The black dashed line is the TL of case S1. All these cases exhibit the almost identical TL behavior at $f < 0.030$ beyond which large variation in terms of peak frequencies and magnitudes are observed. When $L_B \leq L_p$, the transmission is greatly enhanced at $0.030 < f < 0.050$ followed by a drop in TL before the shoot at $f \sim 0.075$. When $L_B > L_p$, TL starts to drop after the first peaks. Similar drops in TL are also observed by Du et al. [15] who also varied the side walls of cavity to different angles for studying the acoustical effect of the liner under stagnant flow. The HTBs center near $f \sim 0.100$ are persistent with the change in L_B. Generally speaking, the reference case S1 have the widest LTB among these cases, but performance at certain low frequencies are not as good as those with small L_Bs.

The acoustic coefficients and the vibration energy of panels are illustrated in Fig. 18. Similar to case

S1, the panels have little response when $f < f_{L_p,1}$, the first natural frequency. Generally, all the coefficients in non-rectangular cavity illustrate similar trends with those in case S1. Non-rectangular cavity causes shifts of peak frequencies in these coefficients leading to more rapid changes with frequency. These changes can be viewed as the amplification/moderation of the trends in case S1. For instance, $\mathscr{R}$ decreases at $0.030 < f < 0.055$ in case S1 and those in all cases C1 to C4 showed similar trends with a minor shift in frequency. However, no obvious trends are observed for the variation of these coefficients when L_B is increased from 5 (C1) to 15 (C4). The trends of $\mathscr{T}$ remains the opposite to those of $\mathscr{R}$. The absorption peaks are similar in all these cases but some peaks are strengthened especially those at $f > 0.100$. Similarly, $\mathscr{A}$ coincides with the peaks of vibration energy as in other cases. Thus, the resonant panel vibration is strongly related to the absorption peak. The absorption effect is insignificant in these cases except at some resonant panel vibrations. The major mechanism of noise mitigation is still wave canceling. The only exception is the absorption peak at $f = 0.225$ in case C2 which exhibits both small $\mathscr{T}$ and $\mathscr{R}$ but large $\mathscr{A}$. This indicates the weak re-radiation from the panel and the mitigation is most probably the result of high order mode radiation as discussed previously.

Fig. 19 shows the dispersion relations of these cases. They follow the theoretical models including the subsonic and supersonic branches. This implies that the shape of cavity is not crucial in modifying the propagation speed of flexural waves on panel. This also explains little variation of peak absorption frequencies observed in all these cases. Changes in shape of cavity do not alter the basic behaviors of the liner but modify certain panel resonant vibration behaviors. Figs. 20 and 21 reveal the panel response to the incident acoustics. Similar to other cases, the normalized S_{C,v_p} in Fig. 20 comprise high response zones near resonant panel vibrations and the characteristics shifts to high f. The phase ϕ_{C,v_p} exhibits horizontal contours and abrupt change across panel at region with large $\mathscr{R}$ (Fig. 21). It is expected that standing wave patterns are on the panels when $\mathscr{R}$ is large. Similar to previous cases, ϕ_{C,v_p} gradually change across panels when $\mathscr{T}$ is large, i.e. in HTB.

Instantaneous acoustic pressure and panel deflection at frequencies with maximum acoustic coefficients in cases C1 and C4 are chosen to further reveal the noise mitigation mechanism of liners with non-rectangular cavities (Fig. 22 to Fig. 24). When $\mathscr{T}$ is large (Fig. 22), both flexural waves appear to propagate downstream only but acoustic waves inside the cavity behave differently. When $L_B < L_p$ (Fig. 22a to i), all the acoustics

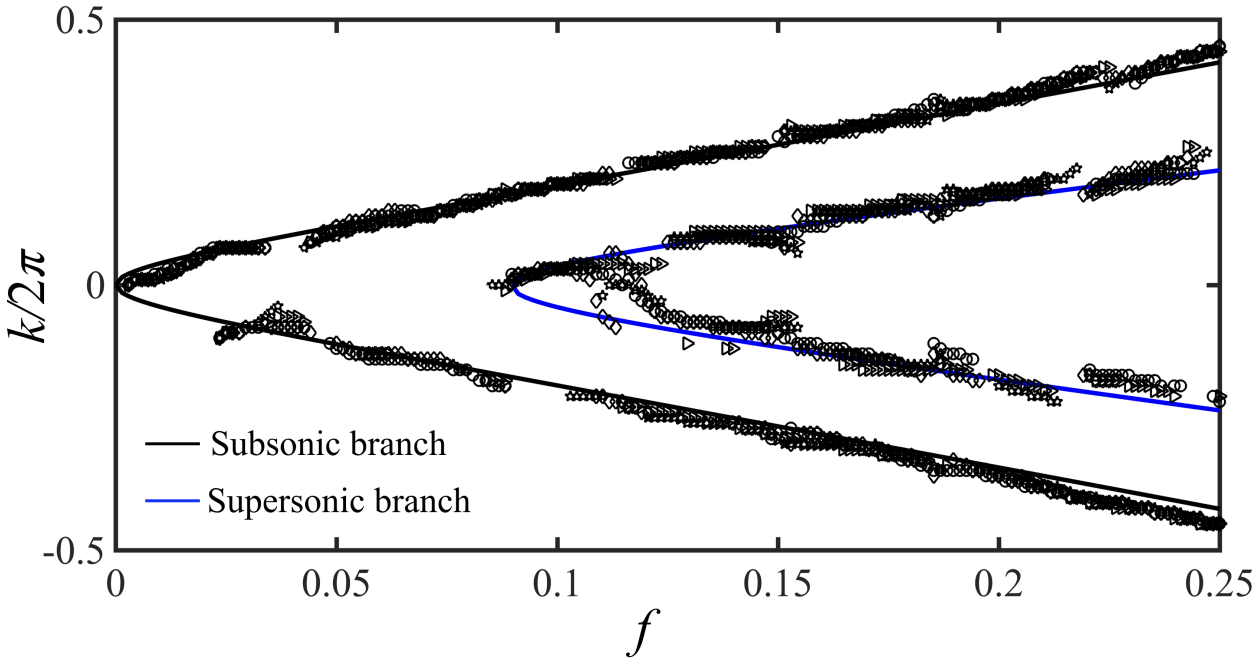

Figure 19: Dispersion relationship of elastic panels with different L_Bs. Black circle: case C1; black diamond: case C2; black triangle: case C3; black star: case C4.

inside cavity seems propagating downstream. However, when $L_B > L_p$ (Fig. 22j to r), the propagation of acoustics inside cavity divides into two regions. The acoustics in the upper quarter ($0 > y > -0.5$) of the cavity propagate downstream while in the lower part ($-0.5 > y > -2.0$) it seems to propagate upstream. The acoustics in these two parts are not in phase. This is probably due to the influence of acute corners at cavity base which creates additional reflections to modify the phase of acoustics near the cavity base. The panels re-radiate weak reflected waves and transmitted waves, but the transmitted waves are almost in phase with the incident acoustics leading to a large $\mathscr{T}$. Although non-planar acoustic waves emerges in the liner region, but only plane waves are able to propagate downstream. The radiated waves by the panel are in phase with the transmitted waves near the ends of the liner such that almost entire incident acoustics is able to propagate downstream.

On the other hand, when $\mathscr{R}$ is large (Fig. 23), both the panel vibration and the acoustics pressure inside the cavity oscillate in standing wave patterns. The panels re-radiate acoustics creating strong upstream and downstream propagating waves. The upstream propagating waves are the reflected waves while those prop-

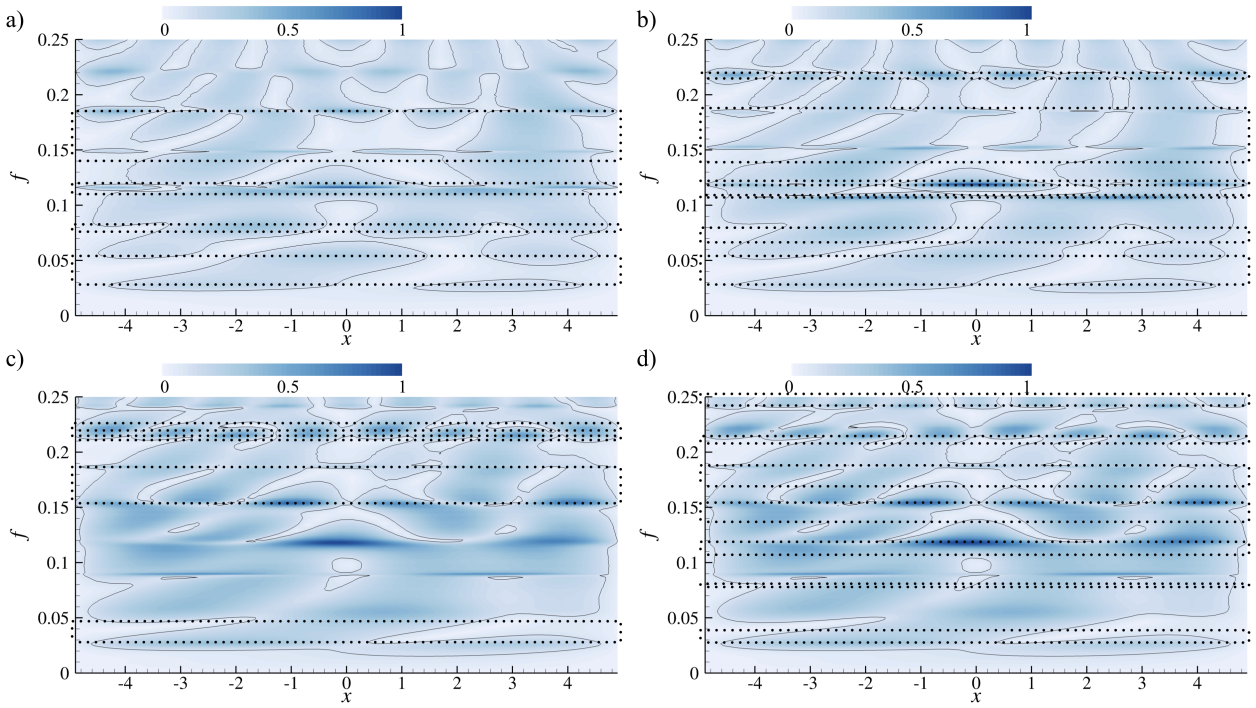

Figure 20: Normalized magnitude of cross power spectral density between p' at probe C and v_p of elastic panels. a) case C1 ($L_B = 5$); b) case C2 ($L_B = 7.5$); c) case C3 ($L_B = 12.5$); d) case C4 ($L_B = 15$).

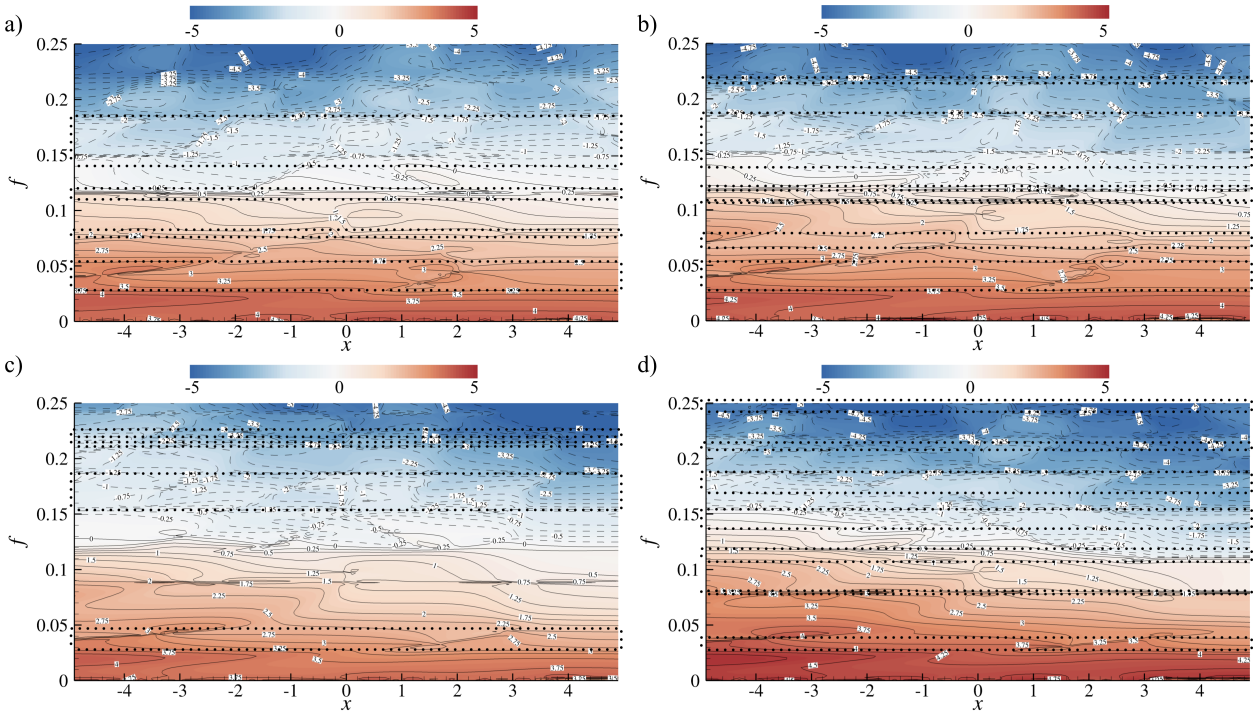

Figure 21: Phase difference between location at probe C and v_p of elastic panels with different L_Bs. a) case C1 ($L_B = 5$); b) case C2 ($L_B = 7.5$); c) case C3 ($L_B = 12.5$); d) case C4 ($L_B = 15$).

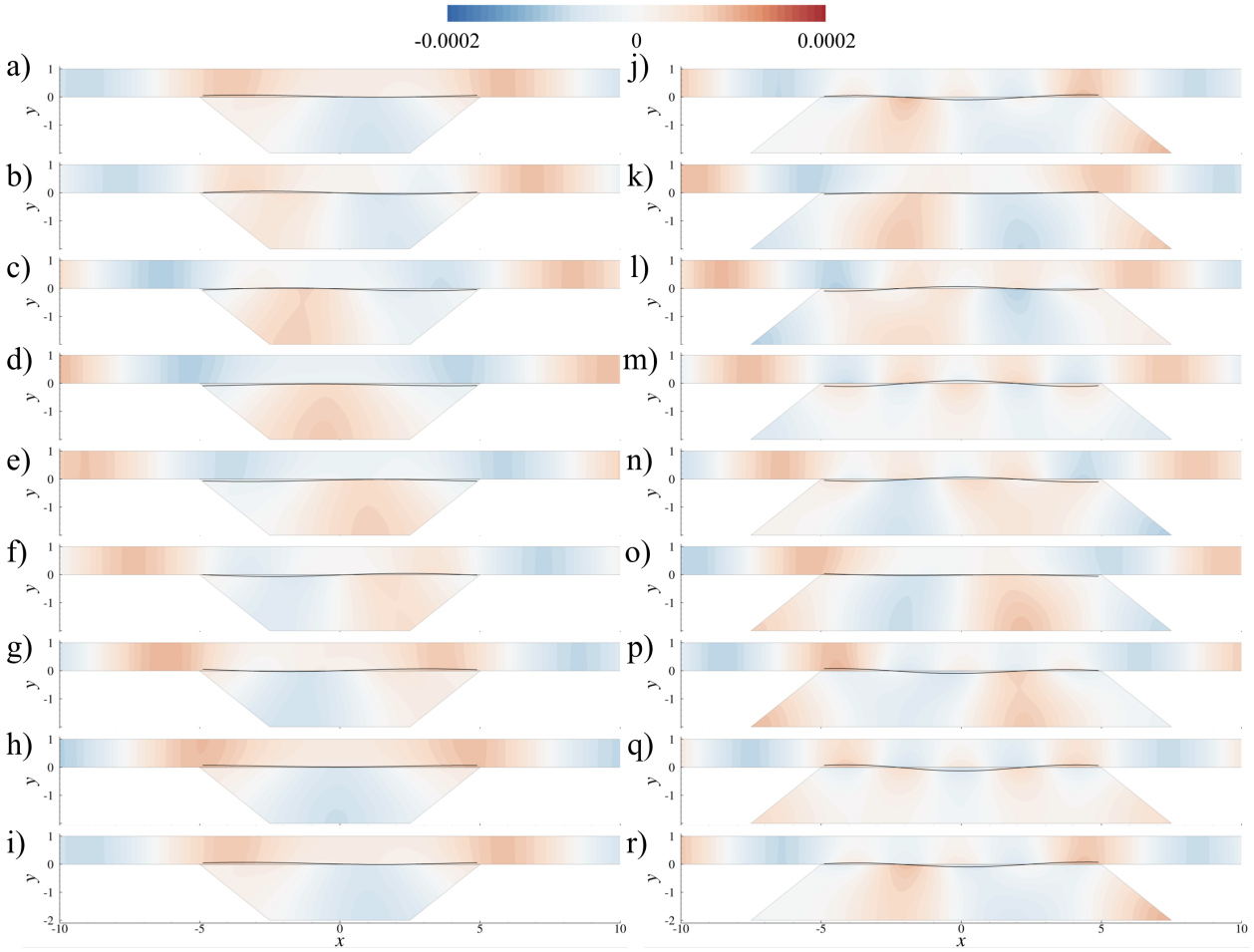

Figure 22: Snapshots of p' and δ distributions (black lines) at large $\mathscr{T}$. a) - i) $f = 0.100$ in case C1; j) - r) $f = 0.127$ in case C4.

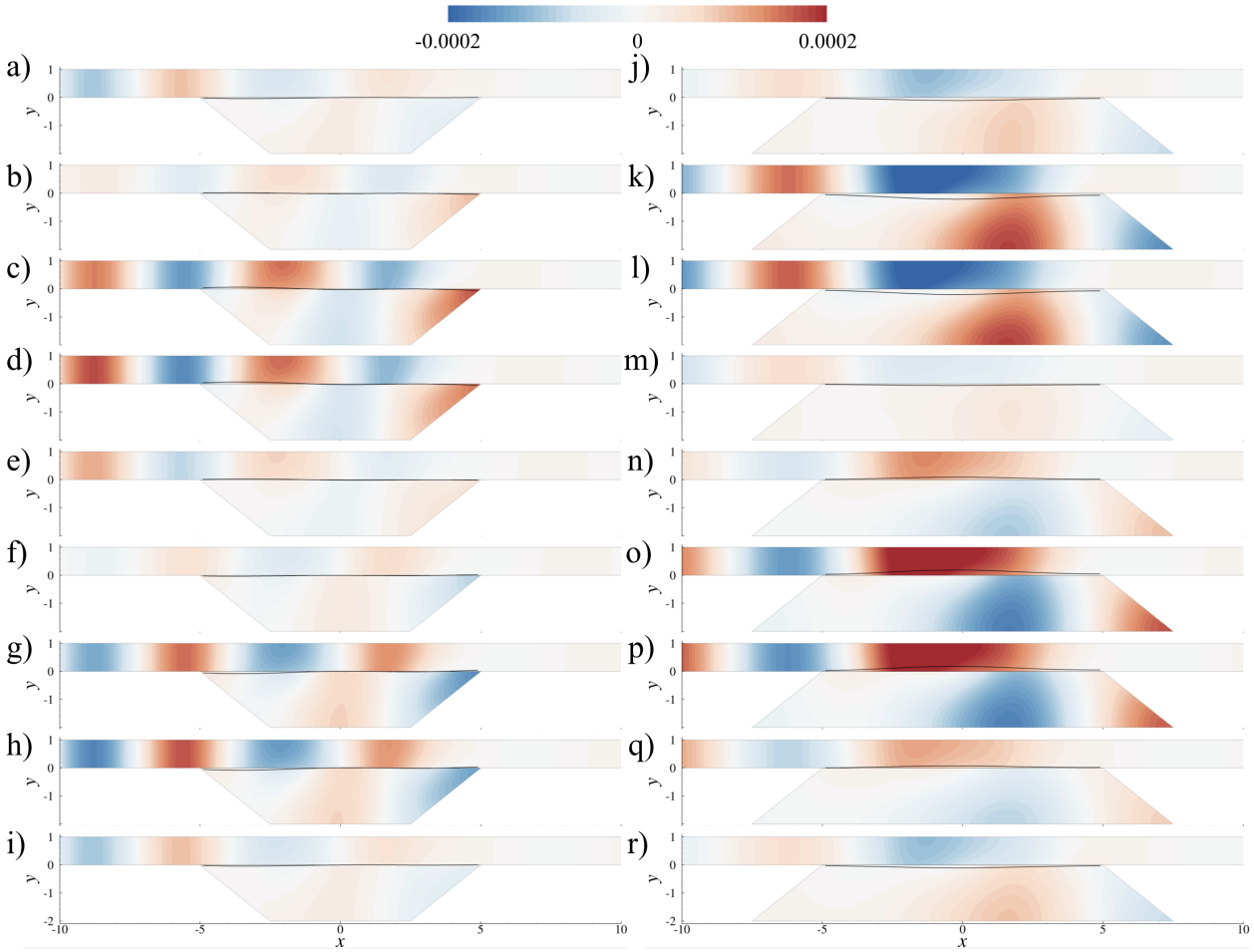

Figure 23: Snapshots of p' and δ distributions (black lines) at large $\mathscr{R}$. a) - i) $f = 0.156$ in case C1; j) - r) $f = 0.116$ in case C4.

agating downstream interferes destructively with the incident acoustics. Only a slight portion of acoustics propagates to the downstream branch. At the frequency $f = 0.156$, the panel in case C1 is in the third resonant vibration mode but anti-nodes and nodes are not uniformly distributed along the panel. Due to the non-rectangular shape of the cavity, the standing wave pattern in the liner region are non-planar in nature. The acute corners of the cavities enhance acoustic modes there in both cases.

Finally, when $\mathscr{A}$ is large (Fig. 24), the acoustics inside cavity and the panel vibration again exhibit standing wave patterns. Similar to other non-rectangular cases, the acoustic modes are non-planar. The re-radiation from panels in general are quite strong in these cases leading to large $\mathscr{R}$. However, depending

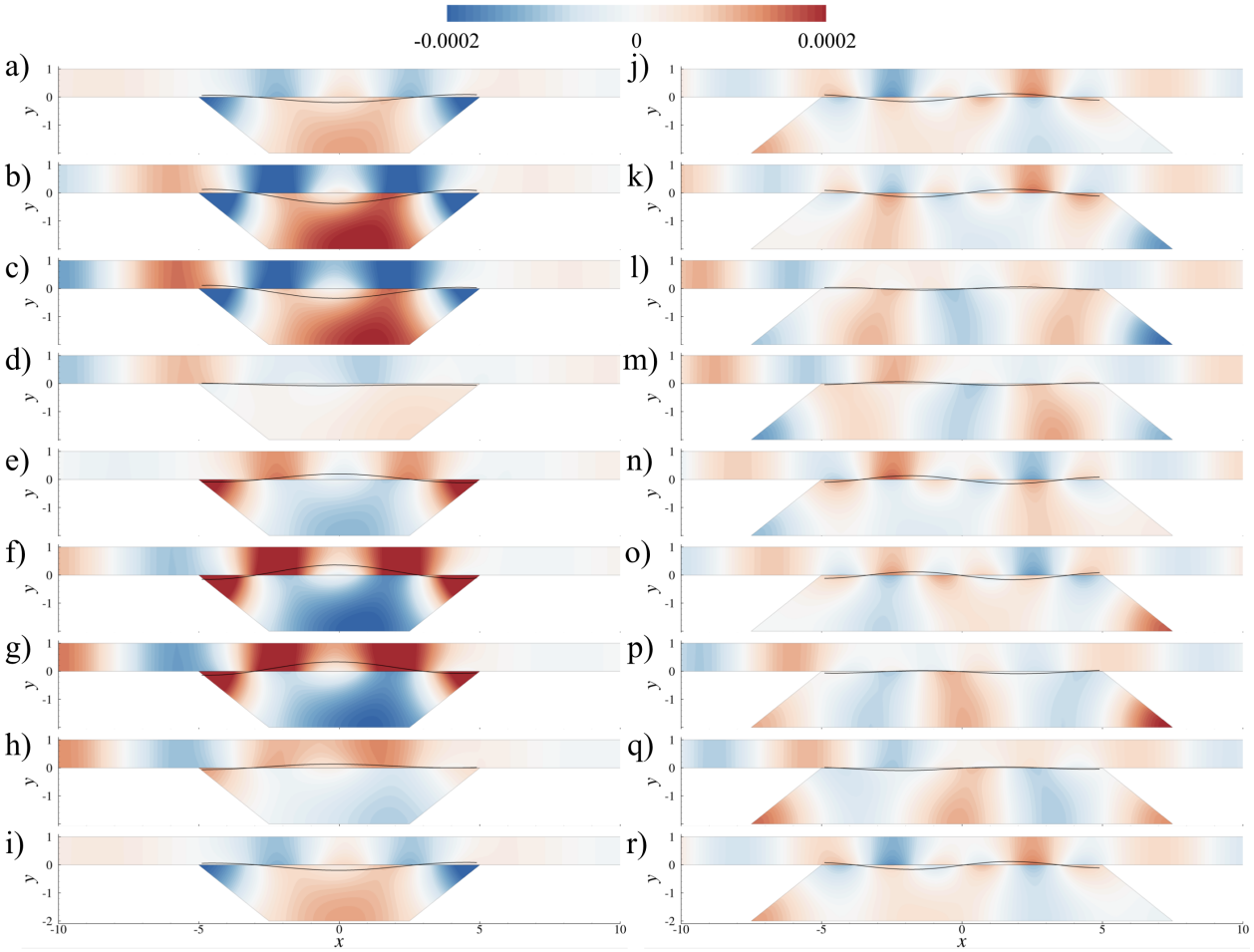

Figure 24: Snapshots of p' and δ distributions (black lines) at large $\mathscr{A}$. a) - i) case C1 ($f = 0.116$); j) - r) case C4 ($f = 0.156$).

on frequency the re-radiation downstream may create destructive interference with the incident acoustics in the downstream branch. This generates a variation in $\mathscr{T}$ among the absorption peaks. Thus, wave canceling is still the dominant mechanism of noise mitigation.

All the numerical results show that the variation of the cavity shape effectively changes the acoustic pressure distribution inside the cavity, which in turn modifies the acoustic re-radiation of the panel. This leads to different levels of noise mitigation across the frequency. The cavity shape change does not offer absolute advantage in noise mitigation as such advantage prevails only at some particular frequencies. Rectangular cavity performs the best among these cases in terms of the LTB size. Nevertheless, all the discussions so far

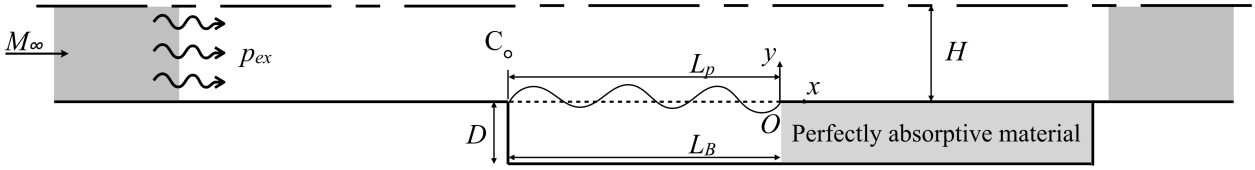

Figure 25: Schematics of numerical domain.

clearly demonstrates the key role of cavity design in the noise mitigation of EP liner which will be further explored in the next section.

3.3. Cavity treatment enhancing liner performance

In previous discussions, two mechanisms of the noise mitigation by EP liner are identified, namely wave canceling and loss of acoustical energy through high mode re-radiation by panel. The wave canceling is dominant in the low frequency noise mitigation except some particular resonant panel vibration at high frequencies. The findings confirm the important role of cavity in the mechanisms which change the acoustic pressure distribution and thus the interference between the acoustic radiation by panel and the incident acoustics.

Inside the cavity, only acoustics are present as the flow is separated by the elastic panel. This is comparatively easier to take the cavity interior as a good spot for acoustic treatment to further enhance the capability of nose mitigation of EP liner as such way is free from the intrusion of duct flow. Similar approach was attempted by Huang [10]. In his work, the cavity was filled fully with porous material for dampening the noise inside the cavity but his results did not show any benefit in overall noise mitigation. This is perhaps due to his assumptions made in the cavity acoustics. He assumes the porous material inside cavity act as compliant support to the vibrating panel. This creates a large difficulty in the modeling because the interface condition between the porous material and the panel may not be realistically represented. In the present study a novel alternative concept is attempted (Fig. 25). Absorptive material is placed downstream end of the cavity rather than beneath panel. The acoustics radiated by the panel inside the cavity is allowed travel to absorptive material for effective dissipation. In order to demonstrate the feasibility of concept, a perfectly absorptive material is firstly attempted. This perfectly absorptive material is modeled by a numerical buffer zone that is adopted originally for minimizing the wave reflected at the inlet and outlet of the numerical

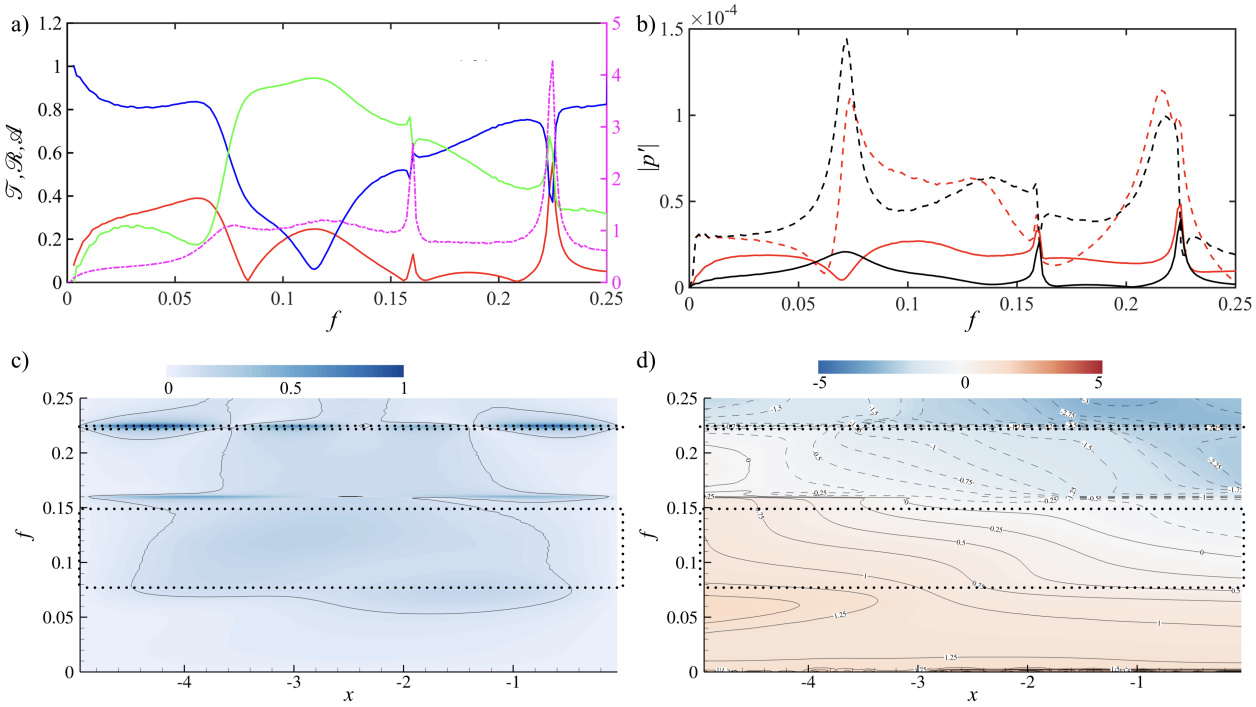

Figure 26: Results of EP liner with cavity comprising of perfectly absorptive material. a) Transmission coefficient $\mathscr{T}$ (blue line), reflection coefficient $\mathscr{R}$ (red line), absorption coefficient $\mathscr{A}$ (green line) and vibration energy (magenta dashed line); b) Acoustic propagation along the line $y = -0.4$ inside cavity in S4 (dashed lines) and cavity with absorptive material (solid lines); $+/-x$ propagation are marked with red lines and black lines respectively; c) Normalized magnitude of cross power spectral density between p' at probe C and v_p of elastic panels ; d) Phase of cross power spectral density between probe C and v_p of elastic panel, ϕ_{C,v_p}.

domain. In this study, settings of case S4 is used with the addition of perfectly absorptive material inside cavity.

The acoustics coefficients are determined to assess the effectiveness of such configuration. Fig. 26a shows these coefficients together with the vibration energy of panel. The transmission is overall weakened as a smaller $\mathscr{T}$ is observed in the entire frequency range compared to that of case S4. The major LTB is slightly shifted from $0.072 < f < 0.143$ to $0.078 < f < 0.149$. $\mathscr{T}$ also changes smoothly over the frequency except near the resonant panel vibration. The effect of the perfectly absorptive material dominates on the reflection and absorption. Regarding the reflection, $\mathscr{R}$ is smaller than 0.4, except at the absorption peak ($f = 0.224$) in this configuration, which is generally much lower than that in case S4. Its behavior also varies with absorption to certain extent rather than with the transmission, notably the matching of peaks in $\mathscr{R}$ and $\mathscr{A}$.

This is totally different from case S4 in which the trends transmission is opposite to that of reflection and the LTB is consistently associated with large $\mathscr{R}$. This observation provides a further evidence that the acoustic distribution inside the cavity has a great effect on the strength of the acoustic radiation by the panel. On the other hand, the absorption is greatly enhanced in the interested frequency range. $\mathscr{A}$ (green line) in the LTB is even higher than those at resonant panel vibration. Fig. 26b shows wave propagations inside the cavity which are also determined with multiple microphone method. The acoustic pressure inside cavity in case S4 are much stronger than that with absorptive material in both $\pm x$ directions. In case S4, the magnitude in $-x$ direction is larger than that in $+x$ direction over some frequency bands. In addition with absorptive material installed, the panel re-radiates in all directions but the radiation is not synchronized over entire panel due to asynchronous nature of panel vibration in this case. For example, the upstream part of panel in deflected downwards compressing the air in cavity while the downstream part of panel deflected upwards relaxing the air there at the same time instant (Fig. 27c). As a result, the acoustic pressure in $-x$ direction is not zero, but it is still smaller than that in $+x$ direction over almost entire frequency band. This implies that the acoustics inside the cavity are effectively dissipated by the absorptive material rather than reflected back to the duct. Furthermore, the panel only responds strongly near the resonance as shown in S_{C,v_p} (Fig. 26c) suggesting a weak re-radiation from the panel as a result. This observation is also consistent with the small $\mathscr{R}$ in Fig. 26a. In Fig. 26d, the phase ϕ_{C,v_p} varies smoothly along the panel even at frequencies with very low transmission. This agrees with previously discussed cases that horizontal contours are associated with large $\mathscr{R}$. Sudden phase change across frequency still exists near the resonant panel vibration.

Figure 27 shows the snapshots of acoustic distribution with the panel deflection at selected peaks in $\mathscr{T}$ and $\mathscr{A}$. The case with local peaks of $\mathscr{R}$ is omitted because $\mathscr{R}$ are small compared to other acoustics coefficient. In case of large transmission at $f = 0.061$ shown in Fig. 27a to Fig. 27i, the panel radiates weak acoustics back to the cavity and duct after being excited by the incident acoustics. Inside the cavity, the acoustics propagate both upstream and downstream. The upstream propagating acoustics are then reflected by the rigid cavity wall and then travel downstream at which no reflection is observed. The scenario is similar to the panel facing an effectively open space due to the fact that the cavity acoustics can leave the liner directly yet without affecting the panel vibration. As such, acoustical energy is also lost through the dissipation by the absorptive material. Fig. 27j to Fig. 27r illustrates the acoustic behavior when the absorption is large

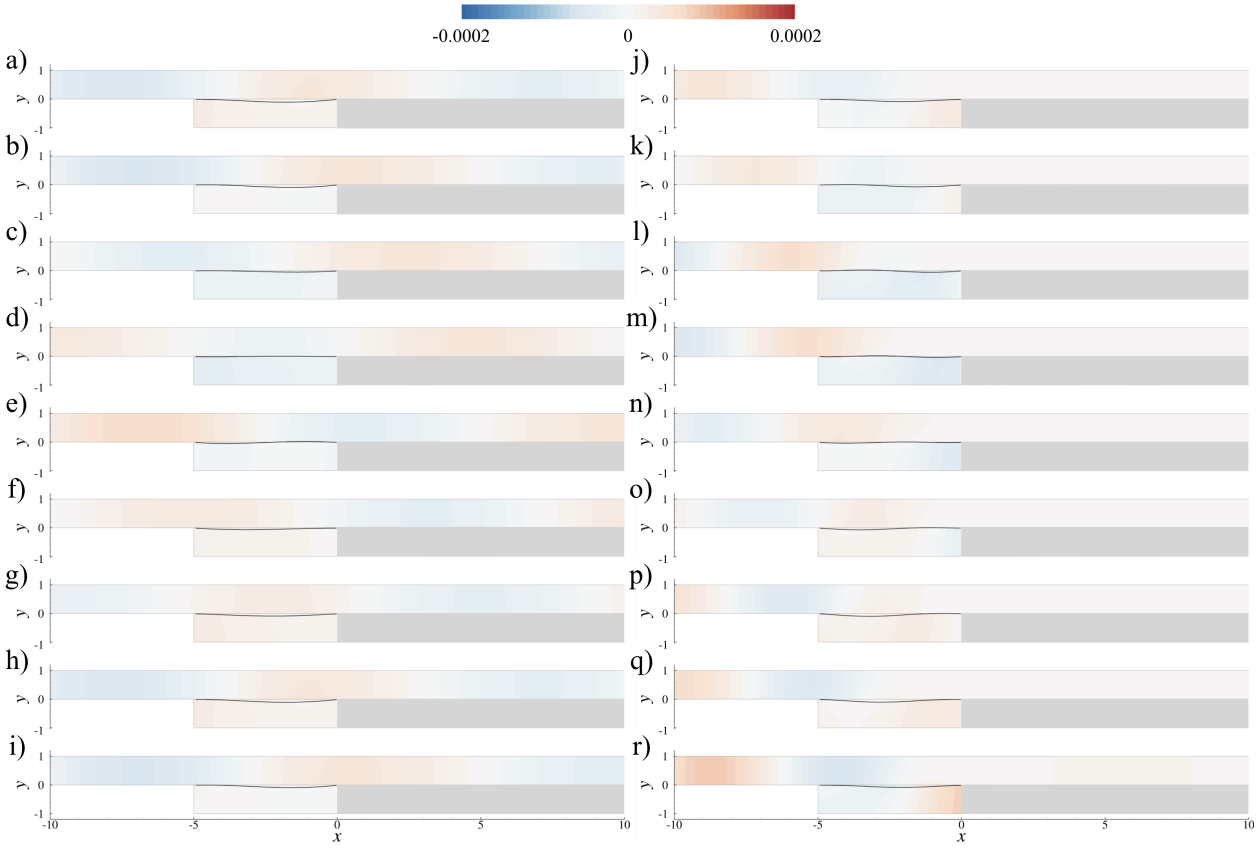

Figure 27: Snapshots of p' and δ distributions (black lines) with the addition of perfectly absorptive material. Grey zones indicate perfectly absorptive materials. a) - i) Large transmission at $f = 0.061$; j) - r) Large absorption (non-resonance) at $f = 0.115$;.

($f = 0.115$). Contrary to absorption in previously reported cases, the flexural wave propagates in opposite directions on panel but the acoustics inside the cavity propagates only towards the absorptive material with no observable reflection. In this way, acoustical energy is lost via dissipation by the absorptive material inside the cavity rather than via wave canceling as indicated by weak reflected waves in duct. Furthermore, it is unlikely that high order mode re-radiation by the panel plays a significant role in noise mitigation because the vibrating energy spectrum shown in Fig. 26a is smaller than those in previously reported cases.

With the introduction of perfectly absorptive material inside the cavity, it is demonstrated that the acoustics radiation by the panel inside the cavity are dissipated completely. The absorptive material to release acoustic pressure away from the liner in an indirect yet effective manner. This action leads to an even

weaker re-radiation from the panel to the duct than that in its counterpart case S4. Without the absorptive material, all panel radiations are all transmitted back to the duct such that either transmitted wave or reflected waves are very strong. Strong reflected wave also may not be desired in certain practical situations. For instance, the reflected waves can create additional nuisance in other locations linked with ventilation systems. This shows the concept is a promising approach in enhancing EP liner in practical applications.

4. Conclusions

The paper reported a numerical study of the effect of back cavity configuration on the performance of elastic panel liner using a time-domain direct aeroacoustic simulation approach which is seamlessly coupled to panel dynamics. The mechanisms of noise mitigation are explored with extensive cross spectral analyses of numerical results obtained from a parametric study of variation in cavity size and shape. In contrast with literature which suggests resonant panel vibration as the main cause of noise mitigation, the dominant mechanism of elastic panel liner is found to be wave canceling, even with resonant panel vibration, in which the noise mitigation relies on the interference between the incident acoustics and the acoustic re-radiation by panel towards the downstream branch. Another mechanism at play is the absorption due to resonant panel vibration. Energy loss occurs during the radiation of high order modes by panel but it does not play a significant role at most of the frequencies of interest in the present study. Though panel structural damping is ignored in the present study, it is expected that its introduction will only enhance noise mitigation rather than generating additional liner self-noise. According to Carpenter and Garrad [28], the effect of introducing structural damping strongly weaken the fluid-structural interaction, i.e. the panel vibration while slightly destabilizes the Tollmien–Schlichting type instabilities that is usually rather weak in the flow-duct with elastic panel liner. However, it is worth further investigation relating the structural damping.

The variation of cavity size effectively changes the acoustic distribution inside the cavity and thus the acoustic re-radiation by the panel. This eventually leads to shifts in the effective working frequency ranges of the liner. When the cavity is very thin, the dynamical response of air inside becomes so stiff that the flexural wave speeds are modified that its supersonic branch emerges at a much higher frequency than the theoretical solution. In this case, the panel responses to the acoustic excitation are strongly weakened except at its resonance. On the other hand, the acoustic distribution inside the cavity can be modified by

the cavity shape. Inside non-rectangular cavity, the acoustics are all in non-planar propagating or standing wave mode. This makes it rather difficult to achieve effective destructive interference between the incident acoustics and the panel acoustic re-radiation, so the noise mitigation performance with these cavities are degraded gently. All these observations clearly pinpoints that the back cavity of elastic panel liner plays a significant role in liner noise mitigation. To further explore the possibility of mitigation enhancement, a new cavity configuration with absorptive material placed at downstream side of cavity is designed and studied. Stronger absorption and less reflection than its ordinary counterpart are attained. The overall transmission is also greatly weakened. This achievement evidently illustrates that the configuration of back cavity is an important consideration for designing mitigation performance of elastic panel liner.

Acknowledgements

The authors gratefully acknowledge the support from the Research Grants Council of the Government of Hong Kong Special Administrative Region under grant number A-PolyU503/15 and the ANR/UGC international FlowMatAc number ANR-15-CE22-0016-01. The second author is grateful to a generous research donation from Philip K. H. Wong Foundation under grant number 5-ZH1X.

References

[1] K. U. Ingard, Notes on Sound Absorption Technology, Noise Control Foundation, New York, 1994.

[2] M. Åbom, S. Allam, On the use of micro-perforates for machinery and vehicle noise control, The Journal of the Acoustical Society of America 132 (3) (2012) 1887–1887. doi:10.1121/1.4754921.
URL http://asa.scitation.org/doi/10.1121/1.4754921

[3] Y. Aurégan, M. Farooqui, J.-P. Groby, Low frequency sound attenuation in a flow duct using a thin slow sound material, The Journal of the Acoustical Society of America 139 (5) (2016) EL149–EL153. arXiv:1606.01877, doi:10.1121/1.4951028.
URL http://asa.scitation.org/doi/10.1121/1.4951028

[4] L. Huang, A theoretical study of duct noise control by flexible panels, The Journal of the Acoustical Society of America 106 (4) (1999) 1801–1809. doi:10.1121/1.427930.
URL http://asa.scitation.org/doi/10.1121/1.427930

[5] X. Yu, Z. Lu, L. Cheng, F. Cui, Vibroacoustic modeling of an acoustic resonator tuned by dielectric elastomer membrane with voltage control, Journal of Sound and Vibration 387 (2017) 114–126. doi:10.1016/j.jsv.2016.10.022.
URL https://linkinghub.elsevier.com/retrieve/pii/S0022460X16305557

[6] S. Choi, Y.-H. Kim, Sound-wave propagation in a membrane-duct (L), The Journal of the Acoustical Society of America 112 (5) (2002) 1749–1752. doi:10.1121/1.1509761.

[7] P. Doak, Excitation, transmission and radiation of sound from source distributions in hard-walled ducts of finite length (I): The effects of duct cross-section geometry and source distribution space-time pattern, Journal of Sound and Vibration 31 (1) (1973) 1–72. doi:10.1016/S0022-460X(73)80249-4.
URL https://linkinghub.elsevier.com/retrieve/pii/S0022460X73802494

[8] L. Huang, Modal analysis of a drumlike silencer, The Journal of the Acoustical Society of America 112 (5) (2002) 2014–2025. doi:10.1121/1.1508778.

[9] L. Huang, Parametric study of a drum-like silencer, Journal of Sound and Vibration 269 (3-5) (2004) 467–488. doi:10.1016/S0022-460X(02)01642-5.
URL https://linkinghub.elsevier.com/retrieve/pii/S0022460X02016425

[10] L. Huang, Broadband sound reflection by plates covering side-branch cavities in a duct, The Journal of the Acoustical Society of America 119 (5) (2006) 2628–2638. doi:10.1121/1.2186431.
URL http://asa.scitation.org/doi/10.1121/1.2186431

[11] Y. S. Choy, L. Huang, Effect of flow on the drumlike silencer, The Journal of the Acoustical Society of America 118 (5) (2005) 3077–3085. doi:10.1121/1.2047207.
URL http://asa.scitation.org/doi/10.1121/1.2047207

[12] H. K. H. Fan, R. C. K. Leung, G. C. Y. Lam, Numerical analysis of aeroacoustic-structural interaction of a flexible panel in uniform duct flow, The Journal of the Acoustical Society of America 137 (6) (2015) 3115–3126. doi:10.1121/1.4921285.
URL http://scitation.aip.org/content/asa/journal/jasa/137/6/10.1121/1.4921285

[13] H. K. H. Fan, G. C. Y. Lam, R. C. K. Leung, Numerical Study of Nonlinear Fluid-Structure Interaction of an Excited Panel in Viscous Flow, in: Flinovia - Flow Induced Noise and Vibration Issues and Aspects - II, Springer International Publishing, Cham, 2019, pp. 253–269.

[14] C. Wang, L. Huang, Time-domain simulation of acoustic wave propagation and interaction with flexible structures using Chebyshev collocation method, Journal of Sound and Vibration 331 (19) (2012) 4343–4358. doi:10.1016/j.jsv.2012.05.015.
URL https://linkinghub.elsevier.com/retrieve/pii/S0022460X12003823

[15] J. Du, Y. Liu, Y. Wang, G. Wang, Vibro-acoustic analysis of an elastically restrained plate duct silencer backed by irregular acoustical cavity, Applied Acoustics 138 (March) (2018) 60–71. doi:10.1016/j.apacoust.2018.03.004.
URL https://doi.org/10.1016/j.apacoust.2018.03.004

[16] G. C. Y. Lam, R. C. K. Leung, K. H. Seid, S. K. Tang, Validation of CE/SE Scheme in low Mach number direct aeroacoustic simulation, International Journal of Nonlinear Sciences and Numerical Simulation 15 (2) (2014) 157–169. doi:10.1515/ijnsns-2012-0118.
URL http://www.degruyter.com/view/j/ijnsns.ahead-of-print/ijnsns-2012-0118/ijnsns-2012-0118.xml

[17] H. K. H. Fan, R. C. K. Leung, G. C. Y. Lam, Y. Aurégan, X. Dai, Numerical coupling strategy for resolving In-duct elastic panel aeroacoustic/structural interaction, AIAA Journal 56 (12) (2018) 5033–5040. doi:10.2514/1.J057324.
URL https://arc.aiaa.org/doi/10.2514/1.J057324

[18] G. C. Y. Lam, R. C. K. Leung, S. K. Tang, Aeroacoustics of T-junction merging flow, The Journal of the Acoustical Society of America 133 (2) (2013) 697–708. doi:10.1121/1.4773351.

[19] G. C. Y. Lam, R. C. K. Leung, S. K. Tang, Aeroacoustics of duct junction flows merging at different angles, Journal of Sound and Vibration 333 (18) (2014) 4187–4202. doi:10.1016/j.jsv.2014.04.045.
URL http://linkinghub.elsevier.com/retrieve/pii/S0022460X14003319

[20] S.-h. Jang, On the multiple microphone method for measuring in-duct acoustic properties in the presence of mean flow, The Journal of the Acoustical Society of America 103 (3) (1998) 1520–1526. doi:10.1121/1.421289.

[21] J. Dugundji, E. Dowell, B. Perkin, Subsonic flutter of panels on continuous elastic foundations, AIAA Journal 1 (5) (1963) 1146–1154. doi:10.2514/3.1738.

[22] R. D. Blevins, Formulas for natural frequency and mode shape, 1st Edition, Van Nostrand Reinhold, New York, 1979.

[23] Y. Aurégan, Ultra-thin low frequency perfect sound absorber with high ratio of active area, Applied Physics Letters 113 (20). doi:10.1063/1.5063504.

[24] M. E. D'Elia, T. Humbert, Y. Auregan, J. Golliard, Optical Measurements of the Linear Sound-Flow Interaction above a Corrugated Plate, in: 25th AIAA/CEAS Aeroacoustics Conference, no. May, American Institute of Aeronautics and Astronautics, Reston, Virginia, 2019. doi:10.2514/6.2019-2716.
URL https://arc.aiaa.org/doi/10.2514/6.2019-2716

[25] D. G. Crighton, The 1988 Rayleigh medal lecture: Fluid loading-The interaction between sound and vibration, Journal of Sound and Vibration 133 (1) (1989) 1–27. doi:10.1016/0022-460X(89)90983-8.

[26] D. C. Ghiglia, L. A. Romero, Robust two-dimensional weighted and unweighted phase unwrapping that uses fast transforms and iterative methods, Journal of the Optical Society of America A 11 (1) (1994) 107. doi:10.1364/JOSAA.11.000107.
URL https://www.osapublishing.org/abstract.cfm?URI=josaa-11-1-107

[27] P. M. Morse, K. U. Ingard, Theoretical acoustics, Princeton University Press, 1986.

[28] P. W. Carpenter, A. D. Garrad, The hydrodynamic stability of flow over Kramer-type compliant surfaces. Part 1. Tollmien-Schlichting instabilities, Journal of Fluid Mechanics 155 (1985) 465. doi:10.1017/S0022112085001902.